# Role of $CO_2$ in low to medium enthalpy geothermal systems in the Central Betic Cordillera (Spain)

C. Lix [1,2]*, P. Zuddas[2], X. Guichet[1], J. Benavente[3], J.A. Luque-Espinar[4], and M. Barbier[1]

[1] IFP Energies Nouvelles, 1 et 4 avenue de Bois-Préau, 92852 Rueil-Malmaison, France

[2] Sorbonne Université, CNRS-INSU, Institut des Sciences de la Terre Paris, ISTeP UMR 7193, F-75000 Paris, Campus Pierre et Marie Curie - 4 place Jussieu 75005 Paris, France

[3] Departamento de Geodinámica e Instituto de Investigación del Agua, Universidad de Granada, Avenida de la Fuente Nueva S/N C.P. 18071- Granada, Spain

[4] Instituto Geológico y Minero de España, Urb. Alcázar del Genil, 4-Edif. Zulema, Bajo., 18006 - Granada, Spain

Corresponding author: Claire Lix

# Role of $CO_2$ in low to medium enthalpy geothermal systems in the Central Betic Cordillera (Spain)


## Abstract

There is growing interest in geothermal energy, which is considered as an efficient energy solution to mitigate rising atmospheric $CO_2$. Besides known high enthalpy geothermal systems, increasing attention is paid to low temperature geothermal systems, as they are suitable for local use. Although geothermal production seems to be an environmentally advantageous renewable energy, it might result in significant $CO_2$ emissions. In this study, we investigate the relationship between temperature, fugacity of $CO_2$ ($fCO_2$), and mineral buffers in the reservoir conditions, taking the low- to medium- enthalpy thermal waters in the Central Betic Cordillera as case study. Using geochemical modeling, three main groups of waters have been identified depending on temperature, buffering mineral assemblage, and $fCO_2$ in their reservoir. A group of waters with a reservoir temperature ranging from 70 to 90°C and located in the intramountain sedimentary basins shows a $fCO_2$ in depth ranging from ~ 6 $x10^{-2}$ and 6 $x10^{-1}$. The reservoir chemistry of this water group seems to be mainly controlled by carbonates and evaporites displaying a $fCO_2$ variation between depth and surface ($\Delta fCO_2$) of $10^{-1}$. Another intermediate group of waters, located in an active extension zone, displays lower temperature (50-60°C) and $fCO_2$ in the reservoir (from $10^{-3}$ to $10^{-2}$). Finally, the third group of waters, located on the metamorphic complexes contacts, show the highest estimated temperatures (130 - 140°C) and $fCO_2$ in the reservoir (1 to $10^{2}$). The two latter groups suggest increasing buffering effect of alumino-silicates, in addition to carbonates and quartz. Therefore, we evidenced a strong relationship between temperature and $fCO_2$ in the reservoir as well as the potential mineral buffers. We discussed the potential of geothermal systems as clean energy source based on the estimation of the $CO_2$ emissions generated by the investigated thermal systems for a practical case of household heating.

## 1 Introduction

Geothermal energy has been widely developed across Europe and the World for the last 50 years, with main focus on the conventional high-temperature geothermal reservoirs. Nevertheless, low (30°C to 100°C) to medium (100 – 150°C) enthalpy geothermal systems have been recently subject to increasing interest (Blasco et al., 2017; Capecchiacci et al., 2015; Fusari et al., 2017) as they may be easily exploited for ground-source heat pump or greenhouses (Battistel et al., 2016). In the current context of global warming and energy transition, geothermal is generally considered to be an environmentally advantageous renewable source of energy. However, emissions of greenhouse gases, and especially $CO_2$, might be generated by geothermal exploitation. Although $CO_2$ release from geothermal electricity production has been shown to be significantly lower than from fossil fuel (Ármannsson, 2003; Hunt, 2001), the efficiency of this energy to mitigate rising atmospheric $CO_2$ is a major concern for societal acceptance. Scientific research programs have been recently dedicated to the development of cost-effective non-carbon emitting geothermal energy (e.g., "Geothermal Emission Gas Control", Horizon 2020, European program). The studies on the $CO_2$ emissions in geothermal systems are mainly dedicated to volcanic geothermal systems (e.g., Ármannsson, 2018; Chiodini et al., 1998; Harvey et al., 2017; Seward and Kerrick, 1996). However, the expansion of the geothermal sector leads to consider a broader range of geothermal resources resulting in possible large $CO_2$ emissions, even in low- and medium- enthalpy geothermal systems.

The $CO_2$ concentration in geothermal waters is strongly related to the geological setting, and more specifically the lithology, of the reservoir. The role of carbonates might be predominant in generation of $CO_2$ as carbonate dissolution or thermal decomposition of carbonates might be major sources of $CO_2$ in fluid whereas carbonate precipitation in the reservoir or in the ascent of the water might be a sink of geothermal $CO_2$. The equilibrium relative to the carbonate minerals and the alumino-silicate minerals, often associated to the

chemical water-rock interactions, is an important parameter to consider as it "buffers" the fluid chemical composition and the $CO_2$ degassing. Therefore, understanding the relationship between the mineral buffer, the fugacity of $CO_2$ ($fCO_2$) (or its partial pressure of $CO_2$, $pCO_2$), and the temperature in the reservoir, is crucial to estimate the $CO_2$ release in geothermal systems. These links between $fCO_2$ and reservoir temperature have been subject to Chiodini and collaborators' investigations since the early 1990's, although they focused mainly on volcanic geothermal systems (e.g., Chiodini et al., 2007, 1998, 1995b)

The Central Betic Cordillera, in the South of Spain, has an interesting geothermal potential with abundant low to medium geothermal resources (Arrizabalaga et al., 2015; Sánchez Guzmán and García de la Noceda, 2010), major fault systems allowing a rapid ascent of the deep hot water (Cerón and López-Chicano, 2002), and moderate-intensity seismic activity. This region is characterized by several occurrences of thermal springs (water with temperature of more than 20°C, according to the average air temperature of this area), known as baños, which have been used, for some of them, as thermal bath since the Roman times. They are mainly exploited for balneotherapy or spa nowadays. The thermal waters in the Central Betic Cordillera are also characterized by large variability in $fCO_2$, and therefore in $pCO_2$. Low $fCO_2$ are observed in the sulfated waters (e.g., Baños Alhama de Granada) whereas large amount of $CO_2$ degassing are known in few springs (e.g., Capuchina de Lanjaron) (Pérez del Villar, 2009). The thermal springs of Baños Alicun de la Torres have been studied as natural analogs for $CO_2$ storage (Prado-Pérez and Pérez del Villar, 2011). Nevertheless, only old Spanish studies have considered globally the thermal waters in the Central Betic Cordillera (Benavente Herrera and Sanz de Galdeano, 1985; Cruz-Sanjulián et al., 1972; Cruz Sanjulián and Granda, 1979). Recent studies (Campos, 2006; López-Chicano et al., 2001a; Prado-Pérez and Pérez del Villar, 2011) characterized the geochemical and hydrogeological properties in specific individual thermal system.

The aim of this study is to evaluate the suitability of the thermal waters for the geothermal exploitation in the Central Betic Cordillera with regard to $CO_2$ emissions. Geochemical and isotopic indicators and thermodynamic calculations can be applied to get insights on the fluid geochemistry, temperature, and $fCO_2$ of the reservoir using the measured physical-chemical characteristics at the surface. The present study attempts to assess the potential mineral assemblages buffering the waters in the reservoir and the variations of $fCO_2$ at the regional scale.

## 2 Geological setting

The sampled thermal waters (springs and wells) are located in the central region of the Betic Cordillera with a greater concentration of points in the Granada Basin (

Figure 1). The Central Betic Cordillera is a complex structure, resulting from the convergence of the Iberian and African plates, which can be subdivided into: (1) the non-metamorphic External Zone, (2) the metamorphic Internal Zones, (3) the Neogene basins. The External Zone is separated from the Internal Zone by a major shear zone called the Internal External Boundary Zone (IEBZ) (Sanz de Galdeano, 1990). The Granada Basin is one of the Neogene intramontainous basin in the Central Betic Cordillera, located at the junction between the Internal and External zones.

### 2.1 Tectonic framework

The Central Betic Cordillera is a tectonically active region structured by several crustal faults (Buforn et al., 2004; Sanz de Galdeano and Peláez, 2011). In the NE part of the Granada Basin, the IEBZ, mentioned above, becomes nearly coincident with the so-called Cadiz-Alicante faults system (CAFS,

Figure 1) extending along 550 km across the Betic Cordillera. This fault system forms a

corridor of dextral strike-slip faults generating crustal discontinuities of at least 7 km depth (Sanz de Galdeano, 2008 and references therein). Besides, two main sets of normal faults affect the basement and the sedimentary infilling of the Granada Basin: one set of E-W faults with low angle dip (< 30◦) toward the south and the north; and a second one with NW-SE faults, which dip westward, mainly located in the NE of the basin (Figure 1) (Galindo-Zaldívar et al., 2015; Rodríguez-Fernández and Sanz de Galdeano, 2006). The thermal waters are strongly related to the faults in the Central Betic Cordillera as the thermal systems are convective fracture-controlled systems (Benavente Herrera and Sanz de Galdeano, 1985; Cruz-Sanjulián et al., 1972).

## 2.2 Lithostratigraphy

The material of the Internal Zone corresponds to Paleozoic to Mesozoic metasediments differentiated into three stacked metamorphic complexes, from the top to the base, by different metamorphic degree and structural position: (1) Maláguide, (2) Alpujárride, and (3) Nevado-Filábride. The Alpujárride Complex, well represented in our study area, consists in a series of nappes of Paleozoic-Mesozoic HP/LT metasediments (Azañón et al., 1998; Azañón and Crespo-Blanc, 2000). The base of the nappes consists of Paleozoic graphite mica schists, which are overlain by Permo-Triassic metapelites with layers of meta-sandstones, dolomite, and limestone. These meta-sediments are in turn overlain by middle-upper Triassic marbles with interbedded gypsum layers and Mesozoic pelagic marls forming the top of the nappes (Martín and Braga, 1987; Prado-Pérez and Pérez del Villar, 2011). The HP/LT Nevado-Filábride materials, outcropping in the Sierra Nevada and Sierra Alhamilla, comprise from the base to the top: Paleozoic graphitic schists, Permo-Triassic mica schists associated with metapelites, Triassic dolomite and marbles, and heterogeneous rocks with Jurassic metabasite inclusions (Gomez-Pugnaire et Fernandez-Soler, 1987; Gómez-Pugnaire et al., 2000).

The External Zone forms the northern part of the Granada Basin basement and crops out in Sierra Elvira and Alicún de las Torres. It is mainly composed of Mesozoic sedimentary rocks, with Triassic evaporitic-bearing marls, dolomitic limestones, and interbedded marls (Braga et al., 2003; Sanz de Galdeano and Vera, 1992).

The sedimentary infilling of the Granada Basin ranges from the Miocene to the Quaternary and is composed, from bottom to top, of clayey conglomerates, calcareous sandstones, marls and silts, gypsum/anhydrite (and locally halite), lacustrine limestones, cemented breccias and alluviums (Braga et al., 2003; Corbí et al., 2012).

### 2.3 Sample location

The thermal waters are mainly situated close to major tectonic and geological structures. The sampling points can be gathered into three groups depending of the nature of the geological features:

- The thermal waters related to the metamorphic complexes: Baño Salado de Lanjaron and Capuchina de Lanjaron springs (BSL and CL) are located in the Sierra Nevada along the detachment between Nevado-Filábride and Alpujárride complexes. Baños Alhamilla spring (BAA) is situated further to the east in the Sierra Alhamilla along the same tectonic contact, where it is also close to the trace of an important strike-slip fault of near N30E direction.
- The thermal waters located in the evaporitic basins (Granada Basin and Guadix-Baza Basin): Baños Santa Fe (SF), Baños de la Malahá (BM), and Sondeo Romilla de la Nueva (SRN) are wells situated in the Granada Basin. Baños Alhama de Granada (BAG), Baños Nuevo Alhama de Granada (BNAG), and Sierra Elvira (SE) are springs located in the Granada Basin. SE is also located on the trace of an active fault, belonging to the NW to NNW directed fault system. Baños de Zujar (BZ) and Baños de Alicún de

las Torres (AT) are springs located in the Guadix-Baza Basin, close to the above mentioned IEBZ and CAFS. The springs SE, BZ, and AT are linked by faults to small Subbetic carbonate outcrops.

- The thermal waters linked to the Baños Urquizar Chico (BUC) and Baños Urquizar Grande (BUG) are located within the Valle de Lecrin tectonic graben within the Alpujárride Complex along faults striking N30E, forming the western termination of the Sierra Nevada Massif.

## 3 Material and methods

### 3.1 Water and dissolved gases sampling

Thirteen thermal water samples were collected in the Granada Basin and in the Betic Cordillera, from nine springs and four wells. Two wells were artesian whereas the other water samples were pumped. All water samples were filtered with 0.45 μm membrane filters and samples assigned to trace elements and Al analyses were filtered with 0.2 μm membrane filters. The water samples dedicated to cations, minor elements, and Al analyses were acidified using suprapure nitric acid ($HNO_3$).

Waters were collected by filling 142 mL Pyrex glass bottles to analyze chemical composition of dissolved gases (Capasso and Inguaggiato, 1998; Inguaggiato and Rizzo, 2004; Lix et al., 2018). The glass bottles were sealed under water with silicon/rubber septa to minimize atmospheric contamination (Capasso and Inguaggiato, 1998).

### 3.2 Water analyses

#### 3.2.1 Physical-chemical properties

Physical-chemical parameters of the waters, including temperature, pH, electrical

conductivity (EC), and alkalinity were measured directly on the field. The combination pH electrode was calibrated with three buffer solutions at pH 4.0, 7.0 and 10.0 (25°C) (CertiPUR® Reference material) and the EC electrode with two potassium chloride standard solutions of 1.41 mS/cm and 12.8 mS/cm (25°C) (CertiPUR® Reference material). The uncertainties on the measurements of temperature, pH, and EC were of ± 1°C, ± 0.1, and ± 0.01 mS/cm respectively. Alkalinity was determined by titration with an 0.01M or 0.1M hydrochloric acid solution depending on the encountered alkalinity range and by following the pH evolution with the pH-meter. The equivalent volume was determined with the Gran's method (Gran, 1952) and the analytical error of the alkalinity measurements was of approximatively ± 5%.

#### 3.2.2 Laboratory chemical analyses

The major cations and anions ($Ca^{2+}$, $Mg^{2+}$, $K^{+}$, $Na^{+}$, $SO_4^{2-}$, and $Cl^{-}$) were analyzed by ionic chromatography. The uncertainty on $Mg^{2+}$, $K^{+}$, $Na^{+}$, $SO_4^{2-}$ determination is ± 5 % whereas that on $Ca^{2+}$ and $Cl^{-}$ is estimated to be ± 10%. Minor and trace elements (Ba, Sr, Al, Fe) were analyzed by Inductively Coupled Plasma Optical Emission Spectrometry ICP-OES. The uncertainty on Ba and Sr determination is ± 10 % whereas that on Al is estimated to ± 20 %.The silica concentrations were determined by a spectrophotometric method following the protocol from Centre d'Expertise en Analyse Environnementale du Québec, (2016), suitable for natural groundwater with Si concentration ranging from 0 to 20 mg/l. The total ionic balance does not exceed 8% for all water samples.

### 3.3 Gas analyses

#### 3.3.1 Extraction and analyses of dissolved gases

The extraction of the dissolved gases was carried out following the method described by Capasso and Inguaggiato (1998) and Inguaggiato and Rizzo (2004). A known volume of host

gas was injected into the upside-down glass bottles while drawing out the equivalent water volume through needles. After equilibration for 24 hours, a variable gas volume was extracted for analyses by injecting Millipore water into the glass bottles.

Gas species ($O_2$, $N_2$, $CH_4$, $CO_2$ and He) were analyzed by gas chromatography (Clarus 500, Perkin Elmer instrument with Carboxen 1000 columns with a hot wire detector and a flame ionization detector) using argon as carrier gas. The composition of dissolved gases, expressed in $cc.l^{-1}$ STP (Standard Temperature and Pressure), was calculated taking into account the volume of gas extracted, the volume of water sample, and the solubility of each gas species (Bunsen coefficient in cc gas/l water STP). The composition of bubbling gases was expressed in either %vol or ppm vol. The accuracy to analyze dissolved gases following the method described by Capasso and Inguaggiato (1998) is within 5.0%.

### 3.4 $\delta^{13}C$ of the Total Dissolved Inorganic Carbon (TDIC)

Analyses of $\delta^{13}C$ of Total Dissolved Inorganic Carbon (TDIC) were carried out with the Analytical Precision 2003 (AP2003) mass spectrometer using the method outlined by Capasso et al. (2005) based on chemical and physical stripping. The results were expressed in ‰ vs. V-PDB standard and with standard deviations of $^{13}C/^{12}C$ ratios of ± 0.2‰.

### 3.5 Geochemical calculations and modeling

In this study, the saturation index calculations and geothermometrical modeling were performed with the (version 3-0-6) PHREEQC software (Parkhurst et al., 2013), using the phreeqc thermodynamic database distributed with the code.

#### 3.5.1 Saturation index

A direct thermodynamic modeling of the multi-component system equilibrium has been performed from the composition of the waters and the physical-chemical parameters. The saturation index of waters with respect to possible minerals ($SI_m$) were calculated to test the equilibrium conditions or the departure from equilibrium of the system, following Equation 1:

$$SI_m = \log \Omega_m = \log \frac{\prod^i (\gamma_i [c_i])^{\nu_{im}}}{K_s(P,T)_m} \quad (1)$$

where $[c_i]$ and $\gamma_i$ are the concentration and the activity coefficient of the ion i, $\nu_{im}$ is the reaction coefficient for the ion i and the mineral m, and $K_S(P,T)_m$ is the solubility constant of the mineral m dependent on temperature and pressure.

### 3.5.2 Chemical geothermometers and geobarometers

Chemical geothermometric techniques were used to estimate the theoretical reservoir temperature of the thermal waters. The application of the chemical geothermometers needs to satisfy the basic assumptions that the waters circulating at depth are in chemical equilibrium with the minerals of the host rocks (i.e., $SI_m$ close to 0) and that their elemental contents have not changed significantly during the water ascent to the surface (including precipitation or dissolution of secondary mineral phases or degassing). Numerous chemical geothermometers have been described in the literature, including silica, Na/K, Na/K/Ca, K-Mg (D'Amore et al., 2000 and references therein). The silica geothermometers are the most common in geochemical investigations of geothermal systems, widely used in different contexts around the world (Verma, 2000a). However, the validity of the silica geothermometers, and especially $SiO_2$-quartz geothermometers, have been questioned at low temperatures (< 100°C) (Fournier, 1977; Rimstidt and Barnes, 1980; Verma, 2000a). At those temperatures, quartz precipitation rate is very slow and saturation is rarely achieved (Bjorlykke and Egeberg, 1993; Rimstidt and Barnes, 1980). Nevertheless, these geothermometers might provide consistent results even at low to

medium temperatures (Blasco et al., 2018) and therefore they have been investigated in this study. $SiO_2$-quartz geothermometers from Fournier (1977), Fournier and Potter (1982), Michard (1979) and Verma (2000b) and $SiO_2$-chalcedony geothermometers from Arnórsson et al. (1983) and Michard (1990) were applied for the studied thermal waters. Although cationic (Na/K, Na/K/Ca, K-Mg) geothermometers have been proven efficient in high temperature systems (> 180°C), they are usually considered as unsuitable in low temperature systems due to the different mineral assemblage governing the water chemistry and equilibrium (Blasco et al., 2017; Chiodini et al., 1995a). Due to these limitations, the Na/K, Na/K/Ca and K-Mg geothermometers have not been applied in this study. The Ca-Mg geothermometer, developed in the first place by Marini et al. (1986) and revised by Chiodini et al. (1995a), is more appropriate for low temperature carbonate-evaporitic system and was therefore used here. This geothermometer assumes equilibrium of the waters with calcite, dolomite and anhydrite in the reservoir, which is a reasonable assumption in the investigated area where these minerals are extensively present.

In order to get an estimation of the fugacity of $CO_2$ ($fCO_2$) at depth, the geobarometrical relationship based on the $(HCO_3^-)^2/SO_4^{2-}$ ratio, $fCO_2$, and temperature (Chiodini et al., 1995a) was applied using the following equation:

$$\log \frac{(HCO_3^-)^2}{SO_4^{2-}} = -4.807 + 0.9871 \log pCO_2 + \frac{794.8}{T} - 0.1655 \log \Sigma_{eq} \qquad (2)$$

where $\sum$eq is the sum of equivalents in the waters.

### 3.5.3 Geothermometrical modeling

Another approach to estimate the reservoir temperature consists of simulating the variation of the saturation states with respect to a group of selected minerals, potentially present in the reservoir, to find the temperature at which the saturation indices simultaneously reach equilibrium (Blasco et al., 2018). This method is based on the same assumption as the classical

chemical geothermometers: the thermal waters are in equilibrium with the mineral phases under reservoir conditions. Hence, the most realistic reservoir temperature corresponds to the temperature at which a group of minerals is at equilibrium (Asta et al., 2012; D'Amore et al., 1987; Tole et al., 1993).

Saturation indices were calculated in the temperature interval between the field temperature and 150°C for the following minerals: quartz, chalcedony, anhydrite, dolomite, calcite, Ca-montmorillonite, laumontite, Mg-chlorite, albite, anorthite, K-feldspar, and kaolinite. Due to the imprecision of the thermodynamic databases, the error on the SI at which the equilibrium is reached is considered to be SI = 0 ± 0.25 (D'Amore et al., 1987). This geothermometrical modeling approach estimates the reservoir temperature within an uncertainty of ± 10°C (Tole et al., 1993).

An additional set of geothermometrical simulations has been performed at the end of the study including addition of $CO_2$ to the initial solution to test the hypothesis of $CO_2$ degassing in an open system.

#### 3.5.4 Hydrogeochemical modeling between surface and depth conditions in closed system

In order to assess the geochemistry of the waters at reservoir conditions and the variation of the $fCO_2$ between the reservoir and the surface, we carried out hydrogeochemical simulations in closed systems. In sedimentary environments, the pH and $fCO_2$ of the waters are highly dependent on the interaction with carbonate minerals. Dolomite is particularly important in the Central Betic Cordillera where large amount are present. $CO_2$ generation might occurs during dolomite precipitation as shown by the following reaction:

$$Ca^{2+} + Mg^{2+} + 4\,HCO_3^- \leftrightarrow\ CaMg(CO_3)_{2(s)} +\ 2\,CO_{2(g)} +\ 2\,H_2O$$

The $fCO_2$ in the system might also be controlled by reactions involving alumino-silicates

and carbonates such as the conversion of kaolinite to Mg-chlorite proposed by Coudrain-Ribstein et al. (1998) and Hutcheon et al. (1993):

$$5\ dolomite + kaolinite + quartz + 2\ H_2 0 \leftrightarrow 5\ CO_2 + 5\ calcite + Mg\text{-}chlorite$$

The modeling workflow was run with the PHREEQC code and includes the following three steps:

(1) Saturation calculations were carried out at the outlet temperature ($T_{out}$) and atmospheric pressure ($P_{out}$),

(2) An increase in temperature was simulated up to the temperature of the quartz geothermometer ($T_{qz}$) and the corresponding hydrostatic pressure of the reservoir ($P_{hydro}$) using a geothermal gradient of 30°C/km,

(3) Waters were equilibrated with a set of minerals at $T_{qz}$ and $P_{hydro}$, to test two different hypotheses:

- Equilibrium with dolomite using $CO_{2(g)}$ as an alternative phase to reach the equilibrium,
- Equilibrium with carbonates and alumino-silicates using calcite, dolomite, kaolinite, quartz, Mg-chlorite as mineral assemblage. These minerals are allowed to dissolve or precipitate to reach equilibrium.

The concentrations of chemical species, pH, $CO_2$ fugacity, and SI of minerals were computed during each step of modeling. By comparing the results of the geochemical modeling (Step 3) with the initial surface geochemical characteristics (Step 1), we evaluate the possible mineral assemblages in equilibrium at reservoir conditions.

These geochemical simulations rely on the assumption that the difference in the quartz saturation index ($SI_{quartz}$) during each step of the modeling does not lead to significant change in temperature. Even if $SI_{quartz}$ varies between -0.13 and 1.27, the $H_4SiO_4$ concentration remains

quite constant for all the thermal waters resulting in a change in apparent temperature (δT) lower than 5°C.

## 4 Results

### 4.1 Chemical characteristics of the waters

The investigated thermal waters have outlet temperature ranging from 20 to 50°C, corresponding to low to medium enthalpy waters, and pH values spanning between 5.8 and 7.6 (Table 1). The conductivity of the studied waters shows a large range of values, from 1 to 34 mS/cm, corresponding to total dissolved solids (TDS) values from 0.67 to 18.17 $g.L^{-1}$.

The thermal waters show a large variability in their chemical composition and a relationship can be evidenced between the water-types and their location relative to the geological structures in the Central Betic Cordillera (Figure 2).

The waters located in the graben formed in the Alpujárride Complex and close to the SE-NW faults have a chemical composition of $Ca^{2+}$-$Mg^{2+}$-$SO_4^{2-}$-$HCO_3^-$ type, displaying interaction with both carbonates and sulfates.

The waters in the evaporitic basins are mainly $Ca^{2+}$-$Mg^{2+}$-$SO_4^{2-}$ water-type resulting from clear interaction with evaporitic material and especially calcium sulfate. The samples BAG and BNAG have a higher $HCO_3^-$ content, with a composition close to the samples from the graben in the Alpujárride Complex. The composition of the BZ water also differs from the others with a $Ca^{2+}$-$Na^+$-$K^+$-$SO_4^{2-}$-$Cl^-$ water-type, showing significant interaction with evaporitic and detrital material.

The thermal waters located at contacts between metamorphic complexes display larger dispersion in their chemical composition. The samples BSL and CL are $Na^+$-$Cl^-$ type whereas BAA is $Na^+$-$Cl^-$-$HCO_3^-$ type.

## 4.2 Saturation indices

The results of the saturation indices calculations at the outlet temperature are shown in Table 2. The waters are mainly close to equilibrium or slightly oversaturated with respect to calcite and dolomite whereas they are undersaturated with respect to gypsum, anhydrite, and halite. However, the thermal waters of AT and BSL display slight undersaturation to undersaturation with respect to the carbonate minerals (calcite and dolomite). Waters are oversaturated with respect to quartz and close to equilibrium with respect to chalcedony. Concerning the saturation indices with respect to alumino-silicates, the waters are oversaturated with respect to kaolinite and Ca-montmorillonite whereas they display large range of saturation with respect to K-feldspar and albite, spanning from undersaturated to highly oversaturated, independently of the relationship with the tectonic structures. The saturation indices of the waters with respect to the considered minerals are pH-dependent and therefore dependent of possible $CO_2$ degassing of the thermal waters.

## 4.3 $CO_2$

Dissolved $CO_2$ concentrations range from 9.51 to 597.5 cc/L, corresponding to $fCO_2$ spanning from 0.02 to 0.78, i.e $pCO_2$ from 0.02 to 0.78 atm (Table 3). The water samples characterized by higher amounts of dissolved $CO_2$ display lower pH values, suggesting that $CO_2$ is the main species responsible of water acidity. The high-$CO_2$ springs of CL, BAA and BUG are also characterized by bubbling gases with similar composition as the dissolved gases (Lix et al., 2018).

The $fCO_2$ values obtained from the speciation-solubility calculations at the outlet temperature range from 0.006 to 1.02 (Table 2). The total dissolved inorganic carbon content of the thermal waters and its isotopic composition ($\delta^{13}C_{TDIC}$), listed in Table 3, range from 2.7 x $10^{-3}$ to 6.3 x $10^{-2}$ mol.$L^{-1}$ and from -9.04 to -1.54‰ vs. V-PDB respectively.

Various carbon sources and processes control the $\delta^{13}C$ of the TDIC including: (1) the

371 degradation of organic matter in the soil (of the recharge area), (2) carbonate dissolution, (3)
372 degassing of mantle-derived $CO_2$. Biological degradation processes in soils usually results in
373 $\delta^{13}C$ values ranging from -23‰ and -9‰ (Clark and Fritz, 1997), which is not well
374 representative of the studied samples. Therefore, the $\delta^{13}C_{TDIC}$ values indicate mainly inorganic
375 origin of $CO_2$ although possible mixing with organic carbon sources cannot be rouled out.
376 Discriminating the carbon source between carbonate dissolution and mantle-derived $CO_2$ might
377 be more complex as their $\delta^{13}C$values overlap, He isotopic composition of dissolved and
378 bubbling gases in these thermal waters show however a dominant crustal component (Lix et al.,
379 2018). Purely inorganic origin of $CO_2$ has been considered in these thermodynamical
380 calculations, given the results of $\delta^{13}C$ of the TDIC.
381

382 ## 4.4 Reservoir temperature and pressure

383 ### 4.4.1 Chemical geothermometers and geobarometers

384 The temperatures provided by the silica and Ca-Mg geothermometers are compiled in Table
385 4. The reservoir temperatures estimated with the different $SiO_2$-quartz geothermometers range
386 from 42 to 146°C corresponding to a mean spanning between 51 and 143°C with a relative
387 standard deviation lower than 6°C. The $SiO_2$-chalcedony geothermometers yields lower
388 temperatures ranging from 20 to 115°C. The $SiO_2$-quartz are more reliable than the $SiO_2$-
389 chalcedony geothermometers since quartz might be the phase controlling the dissolved silica in
390 the thermal waters in the Betic Cordillera. Indeed, quartz occurrences and mineralizations have
391 been described in the Internal Zones of the Betic Cordillera as well as in the Neogene basins
392 whereas chalcedony have not been described in mineral assemblages. Although the kinetics of
393 quartz reaction is very slow below 100°C (Rimstidt and Barnes, 1980), the mineral equilibrium
394 approach developed in this study might support the temperatures obtained from quartz
395 geothermometers.

396 The thermal waters located in the evaporitic basins (Granada and Guadix-Baza Basins)
397 show estimated reservoir temperature from $SiO_2$-quartz ranging from 74 to 95°C. Assuming a
398 thermal gradient of 30°C/km, which can be expected in the studied area (Fernàndez et al., 1998),
399 these temperatures would correspond to depths and hydrostatic pressures varying from 2.5 to
400 3.2 km and from 250 to 320 atm respectively. The thermal waters BUC and BUG, located close
401 to the SE-NW faults, show the lowest estimated reservoir temperature, ranging from 51 to 58°C
402 and corresponding to hydrostatic pressure spanning between 170 and 200 atm respectively. The
403 thermal waters located at the contacts between metamorphic complexes (BAA, CL, and BSL)
404 show the highest estimated reservoir temperatures ranging from 126 and 142°C, corresponding
405 to depths of 4 - 4.5 km and a hydrostatic pressures of 400 to 450 atm.
406 The Ca-Mg geothermometer provides temperatures ranging mainly between 71 and 91°C
407 with little variation between the different thermal waters (Table 4). The obtained temperatures
408 are in good agreement with those of $SiO_2$-quartz geothermometers for the waters located in the
409 evaporitic Granada Basin. However, the Ca-Mg geothermometer give similar reservoir
410 temperatures regardless of the geological context of the studied thermal waters, due to low
411 variations in their Ca/Mg ratios, ranging mainly from 1.5 to 2.4. Therefore, it seems that this
412 geothermometer might not be suitable for all investigated thermal waters in the central Betic
413 Cordillera.
414 The results of the geobarometrical method based on the $(HCO_3^-)^2/SO_4^{2-}$ ratio (Chiodini et
415 al., 1995a) give values of fugacity of $CO_2$ ($fCO_2$) in depth ranging from 0.04 to approximatively
416 23. The high values (> 5) are obtained for the thermal waters located on the contact of
417 metamorphic complexes (CL, BSL, and BAA).
418
419 4.4.2 Geothermometrical modeling
420 The first results of the geothermometrical modeling including all mineral phases (quartz,

chalcedony, anhydrite, dolomite, calcite, Ca-montmorillonite, laumontite, Mg-chlorite, and kaolinite) do not reach a common equilibrium temperature (Figures 3 and 4).

Although we can expect the carbonates as part of the buffering mineral assemblage in depth due to their ubiquity in the sedimentary basin and in the Central Betic Cordillera, they cannot reach equilibrium in the reservoir conditions. As shown in Figures 3 and 4, the waters are close to equilibrium or oversaturated with respect to calcite and dolomite in the outlet conditions and these minerals have retrograde solubility. The apparent oversaturation in the outlet conditions might result from $CO_2$ outgassing process and a corresponding increase in pH during the ascent of the waters to the surface.

#### 4.4.3 Hydrogeochemical modeling

The results of the simulations show that, globally, $fCO_2$ in the outlet conditions varies between $6 \times 10^{-3}$ and 1, i.e. $pCO_2$ between ~ $6 \times 10^{-3}$ and 1 atm. The $fCO_2$ obtained in the third step of the simulation after equilibration with dolomite show values ranging from ~ $2 \times 10^{-2}$ and 40 (Figure 5), whereas the values of $fCO_2$ after equilibration with alumino-silicates and carbonates vary between $5.4 \times 10^{-3}$ and $1.8 \times 10^{2}$ (Figure 6). The logarithmic relationship between $fCO_2$ and temperature for the waters equilibrated with the both carbonates and alumino-silicates might reflect strong control by the equilibrium mineral assemblage on the chemical water composition and $CO_2$ content.

The geochemical modeling allows discriminating the three groups of waters, already distinguished by geology, regarding the $fCO_2$ in the reservoir conditions:

- Group of waters located in the evaporitic basins

The results of the simulations in the evaporitic Granada Basin give a pH of the waters in equilibrium with dolomite in the reservoir conditions ($74 < T < 95$°C and $250 < P_{hydro} < 320$

atm) ranging from 6.5 to 6.8 and an estimated $fCO_2$ spanning between $9 \times 10^{-2}$ and $1.6 \times 10^{-1}$ (Figure 5). The simulations taking into consideration carbonates and alumino-silicates give similar ranges of pH (from 6.5 to 6.7) and $fCO_2$ (from $6 \times 10^{-2}$ to $2 \times 10^{-1}$) to those obtained with dolomite equilibrium for the water points located in the Granada basin (Figure 6). However, the two samples BNAG and BZ show slightly higher $fCO_2$ ranging from $3 \times 10^{-1}$ and $6 \times 10^{-1}$. The thermal water of Alicun de las Torres (AT), showing a lower reservoir temperature similar to BUC and BUG samples, have an estimated low $fCO_2$ at depth for both simulations ranging from $1 \times 10^{-2}$ to $3 \times 10^{-2}$ (Figure 5 and 6). The variation in $fCO_2$ between the steps 1 and 3 of the simulation, $\Delta fCO_2$, estimated for this group of thermal waters ranges from $3 \times 10^{-2}$ to $6 \times 10^{-1}$ (Figure 7). This corresponds to a difference in calculated $CO_2$ concentration between the steps 1 and 3 of the simulations ranging from ~ 1 to 5 mmol/L.

- Group of waters in the graben in the Alpujárride complex

The results of the equilibrium simulations with dolomite in the reservoir conditions ($51 < T < 58$°C and $170 < P_{hydro} < 200$ atm) for the waters located in the graben into the Alpujárride Complex give a pH of the waters of approximatively 6.8 and an estimated $fCO_2$ of $6 \times 10^{-2}$ (Figure 5). The simulation of these waters in equilibrium with both carbonates and alumino-silicates (calcite, dolomite, quartz, kaolinite, and Mg-chlorite) give higher values of pH ranging from 7.3 to 7.4 and lower values of $fCO_2$ spanning between $5 \times 10^{-3}$ and $9 \times 10^{-3}$ (Figure 6). The estimated variation in $fCO_2$ between the depth and the surface, $\Delta fCO_2$, ranges from ~ 0 to $6 \times 10^{-2}$ (Figure 7), corresponding to maximum 1 mmol/L of $CO_2$.

- Group of waters located at contact with metamorphic complexes

Both geochemical simulations show high $fCO_2$ values ($> 7 \times 10^{-1}$) and low pH (ranging from 5.1 to 6.7) at reservoir conditions ($126 < T < 142$°C and $400 < P_{hydro} < 450$ atm) for the thermal waters located at the contact with the metamorphic complexes. The estimated $fCO_2$ at

depth is lower considering the equilibrium with dolomite only (ranging from 6 x $10^{-1}$ to 6) than considering the equilibrium with the carbonate and alumino-silicate assemblage (ranging from 25 to 180) (Figures 5 and 6). The estimated $\Delta fCO_2$ for this group of thermal waters spans from 6 x $10^{-1}$ to 1.8 x $10^{2}$ (Figure 7), corresponding to 20 mmol/L to 0.85 mol/L of $CO_2$.

#### 4.4.4 Geothermometrical modeling with $CO_2$ degassing (open system)

- Group of waters located in the evaporitic basins

The geothermometrical simulations with the lowest estimation of $CO_2$ addition deduced from the hydrogeochemical modeling, 1 mmol/L, result in a common reservoir temperature of 75 to 90°C for the waters of the evaporitic basins (Figure 8). Waters are at potential equilibrium with the following mineral buffer: carbonates (calcite and dolomite), anhydrite, quartz, and possibly Mg-chlorite or Ca alumino-silicate (laumontite or a Ca-montmorillonite). These results show that low amounts of $CO_2$ degassing (~ 1 mmol/L) are necessary in an open system to reach the equilibrium with dolomite and alumino-silicates. Evaporites are also part of the buffer mineral assemblage in this sedimentary environment.

- Group of waters in the graben in the Alpujárride Complex

The geothermometrical simulations in an open system with addition of 0.5 mmol/L $CO_2$ show estimated reservoir temperatures ranging from 50 to 60°C for the waters located in the graben in the Alpujárride Complex (Figure 9) with the following mineral buffer: carbonates (calcite and dolomite), quartz, and Ca alumino-silicate (Ca-montmorillonite). Higher amounts of added $CO_2$ do not lead to a common equilibrium of mineral phases at a specific temperature.

- Group of waters located at contact with metamorphic complexes

Modeling of $CO_2$ degassing in an open system with geothermometrical simulations shows that 7 mmol/L to 1 mol/L of added $CO_2$ are necessary for the waters to be at equilibrium at

498 temperature ranging from 120 and 140°C with the following mineral assemblage: quartz and
499 dolomite, and sometimes Mg-chlorite and laumontite (Figure 10).
500

501 **5 Discussion**

502 5.1 Role of the mineral buffers in $CO_2$ estimation

503 The thermal waters in the Central Betic Cordillera are characterized by large heterogeneity
504 in their geochemistry in the outlet conditions and in their geothermal characteristics. The three
505 groups of waters, which were defined based on water composition and geology at the thermal
506 water locations, can be also distinguished by the temperature and $fCO_2$ in the reservoir. The
507 groups of thermal waters have distinct reservoir temperatures, estimated with the SiO2-quartz
508 geothermometer, ranging from low-enthalpy (~55°C) to medium-enthalpy (~140°C)
509 geothermal systems. Using the results of the geochemical and geothermometrical modeling we
510 discuss in this section the mineralogical buffers and chemical properties of the reservoirs and
511 the variations in $fCO_2$ between depth and the surface ($\Delta fCO_2$) in both closed and open system
512 for the three groups of waters. For all groups the assessed $\Delta fCO_2$ indicates $CO_2$ degassing during
513 the ascent of the water to the surface. The equilibrium with respect to mineral phases in the
514 reservoir conditions seems to have a strong control on $CO_2$ release (Figure 7).

515 The group of thermal waters located in the sedimentary basins (Granada and Guadix-Baza
516 Basins), whose reservoir temperatures range from 74 to 95°C, seem to be buffered at depth by
517 mainly carbonates, evaporites, quartz and a few alumino-silicates. The fact that there is a good
518 agreement in $\Delta fCO_2$ with both dolomite buffer and carbonate/alumino-silicate buffer shows that
519 carbonates are the predominant mineral buffer in this environment. The values of $fCO_2$ resulting
520 from geochemical simulations at depth are in quite good agreement with those estimated by the
521 geobarometer from Chiodini et al. (1995a), ranging from 0.04 to 0.16. This geobarometer,

specifically established for low- to medium- geothermal systems hosted in carbonates and evaporites, is certainly an efficient tool to estimate the reservoir $fCO_2$ in this sedimentary context (similar range of temperature and $fCO_2$).

The presence of evaporites needs to be considered for the geothermal systems in sedimentary environment as it might enhance $CO_2$ release through a dedolomitization process. Prado-Pérez and Pérez del Villar (2011) showed that the thermal water AT may result from dedolomitization at depth followed by $CO_2$ degassing. Dedolomitization, which is a process described in other natural systems (Auqué et al., 2009; López-Chicano et al., 2001b), corresponds to dolomite dissolution and calcite precipitation caused by the dissolution of gypsum and/or anhydrite. $CO_2$ loss, before or after outlet of the thermal waters, might occur as evidenced by the presence of fossil and present-day massive thermogenic travertine deposits (Prado-Pérez and Pérez del Villar, 2011) in the Alicun de las Torres site. This process of dedolomitization is most probably occurring in other geothermal systems in the evaporitic Granada and Guadix-Baza basins.

For the thermal waters located in the graben in the Alpujárride Complex, which show the lowest estimated reservoir temperature, the buffer minerals are carbonates, quartz, and Ca alumino-silicate (Ca-montmorillonite). $\Delta fCO_2$ is higher considering the dolomite buffer than considering the carbonate/alumino-silicate buffer. The difference in $fCO_2$ simulated with the two types of mineral buffers (dolomite only and the carbonate/alumino-silicate association) for the thermal waters in the graben might be the signature of the basement, whereas the similar $fCO_2$ estimated for the waters in the sedimentary basin would be the signature of the sedimentary pile. Moreover, the values of $fCO_2$ for both simulations at depth are lower than those estimated by the geobarometer from Chiodini et al. (1995a) of 0.54 and 0.66 for BUC and BUG samples respectively.

On the other hand, for the group of waters located at contact with the metamorphic

complexes, which displays the highest estimated reservoir temperature (130 – 140°C), the mineral buffer assemblage at depth is more difficult to assess due to the large $CO_2$ degassing. Indeed, these waters show the highest measured dissolved $CO_2$ concentrations (> 39 $cm^3/L$) distinguishing them from the other thermal springs in the Central Betic Cordillera. They are at equilibrium with quartz and dolomite, and close to equilibrium with Mg-chlorite and laumontite in the reservoir conditions. The $\Delta fCO_2$ is lower with the dolomite buffer than with the carbonate and alumino-silicate buffer (Figure 7).

The results of the simulations show that $CO_2$ degassing is lower in open system than in closed system, highlighting the importance to evaluate the efficiency of the system to rapidly ascend water from depth to the surface. Calcite precipitation might result from the $CO_2$ degassing process due to pH increase and kinetic constrains compared to dolomite precipitation. The amount of precipitated calcite can be evaluated during a given time range using the amount of $CO_2$ loss during the ascent of the water and the estimated flow rate of the springs found in literature and checked in the field (ranging from 0.2 to 100 L/s). Assuming a time range comprised between 1,000 and 100,000 yr, the amount of calcite precipitated is estimated to range from ~ $10^2$ to $10^6$ $m^3$ for the waters in the basins or their borders. This estimation is in good agreement with the volume of travertines that can be deduced from the study of Martín-Algarra et al. (2003) in the northeastern part of the Granada Basin (from $10^4$ to $10^5$ $m^3$ for the last 200,000 yr).

### 5.2 Relationship between $fCO_2$ and temperature

Using thermodynamic calculations (hydrogeochemical and geothermometrical simulations), we show the key role of the reservoir temperature and the buffer mineral assemblage on the estimation of $fCO_2$ and therefore $pCO_2$. A recent study on the geochemical characterization of geothermal systems pointed out that the $CO_2$ trapping mechanism is mainly

controlled by reservoir temperature (Elidemir and Güleç, 2018). In our studied area, we found increasing reservoir $fCO_2$ with increasing reservoir temperature (Figure 7). The thermal waters with intermediate reservoir temperature (70 to 90°C) show the lowest uncertainty on the variation of $fCO_2$ between depth and the surface ($\Delta fCO_2$) with the two mineral buffers (dolomite only and assemblage of carbonates and alumino-silicates). Higher uncertainty on $\Delta fCO_2$ is observed for the thermal springs with the higher reservoir temperature (120-140°C): carbonates and alumino-silicates buffer predicts higher $\Delta fCO_2$ than dolomite as mineral buffer. The thermal waters with the lowest reservoir temperature also show a large uncertainty in $\Delta fCO_2$ but higher $\Delta fCO_2$ is assessed considering dolomite equilibrium in the reservoir rather than equilibrium with carbonates and alumino-silicates. The results of these highly-simplified mineralogical systems suggest that dolomite tends to equilibrate at low temperature whereas more silicates might be involved at high temperature leading respectively to higher uncertainty in $fCO_2$. The difference in $\Delta fCO_2$ between low and high temperature with respect to the considered mineral buffers might also be interpreted by the large uncertainty in thermodynamic data at the system temperature conditions.

### 5.3 Implications for sustainability of geothermal energy in the Central Betic Cordillera

In order to estimate the environmental impact associated with the $CO_2$ degassing of the investigated thermal waters, the $CO_2$ emissions generated by these thermal systems were estimated for potential household heating purpose and were compared to those produced by a natural gas heating system. The average household energetic consumption (Q) for heating system of a 100 $m^2$ house in Western Europe is 11,600 kWh/yr, equivalent to 4.18 $x10^{10}$ J/yr (Lapillonne et al., 2014).

Using this average household energetic consumption, we can estimate the amount of $CO_2$

597 ($nCO_2$) that would be emitted from a natural gas furnace used to heat a 100 $m^2$ house (Equation
598 3).

$$(n_{CO_2})_{emitted} = (n_{CH_4})_{consumed} = \frac{Q}{HHV} \quad (3)$$

599 where HHV is the higher heating value of methane (891 kJ/mol). Hence, a natural gas furnace
600 would consume 4.69 x $10^4$ mol of $CH_4$ and would hence produce the equal amount of $CO_2$.
601 This value can be then compared to the amount of $CO_2$ that would be produced by the use
602 of the geothermal energy of the thermal springs in the Betic Cordillera area. If we first consider
603 the ideal case of a thermal water with reservoir temperature ($T_{depth}$) equivalent to the maximum
604 temperature of the heating system ($T_{depth} = T_{max} = 60°C$), the amount of water that has to be
605 pumped to heat a 100 $m^2$ house, $n_{water,}$ expressed in mol, can be estimated according to the
606 following equation:

$$n_{water} = \frac{Q}{Cp_{water} * \Delta T} \quad (4)$$

607 where Q is the average value of household energetic consumption, $Cp_{water}$ is the isobaric heat
608 capacity of water and ΔT is the temperature range of the internal heating cycle (20°C with $T_{max}$
609 = 60°C and $T_{min}$ = 40°C).
610 Assuming a constant $Cp_{water}$ of 75.4 J/mol/K and an efficiency of the heat exchanger of 100 %,
611 the necessary quantity of water to heat a 100 $m^2$ house would therefore be 2.77 x$10^7$ mol.
612 We can assess the amount of water that has to be pumped for the two other groups of
613 thermal waters considered earlier with reservoir temperature ($T_{depth}$) of 90 and 140°C using to
614 the following equation:

$$(n_{water})_{pumped} = \frac{Q}{Cp_{water} * (T_{depth} - T_{max})} \quad (5)$$

615 We found that the amount of water that has to be pumped is 1.85 x$10^7$ and 6.15 x$10^6$ mol
616 respectively. Using the average $CO_2$ concentration estimated for each thermal water groups (2
617 x$10^{-4}$, 5 x$10^{-3}$, 8 x$10^{-1}$ mol/L), we can estimate the amount of natural $CO_2$ degassed during

household heating ranging between 1.0 $x10^2$ and 8.9 $x10^4$ mol. The estimated amount of $CO_2$ released from geothermal waters used in heating is lower by 1 to 2 orders of magnitude than the amount of $CO_2$ generated by a natural gas furnace for the two first groups of thermal waters ($T_{depth}$<130°C) (Figure 11). However, similar quantity of $CO_2$ could be released from the thermal waters with the higher $T_{depth}$ as those produced by a natural gas furnace.

These estimations of $CO_2$ emissions in this simple practical application of heating a 100 $m^2$ house show that the geothermal energy is globally a cleaner energy than natural gas but might release as much $CO_2$ as a natural gas furnace in certain conditions (high reservoir temperature and $fCO_2$). These estimations are based on possible gas venting during the heat production, which are usually neglected in life cycle assessment of carbon intensity of geothermal system (McCay et al., 2019).

These estimations, giving us the order of magnitude of $CO_2$ emissions that could be generated by the investigated geothermal systems, lead to explore possible exploitations of the geothermal resource. Direct electricity production (e.g. enhanced geothermal systems) might be considered for the thermal waters with the highest reservoir temperature ($T_{depth}$=140°C) emitting large quantity of $CO_2$. This use would have to be coupled to $CO_2$ capture and storage to make it a renewable and clean energy.

## 6 Conclusions

Our study provides the first characterization of the reservoir conditions (T, P, and geochemistry) for the thermal waters in the central part of the Betic Cordillera. The $fCO_2$ at depth were tentatively assessed with both a chemical geobarometer and direct geochemical simulations. The variation of $fCO_2$ ranges from approximatively 6 x $10^{-3}$ to $10^2$ at the scale of the area. Based on the geology of the thermal water locations and the results of the geothermometrical and thermodynamic geochemical simulations three groups of waters have

643 been determined.

644 The group of the thermal waters located in the sedimentary basin has estimated reservoir
645 temperatures ranging from approximatively 70 to 90°C and $fCO_2$ varying between $6 \times 10^{-2}$ and
646 $6 \times 10^{-1}$. The estimated variations in $fCO_2$ between the depth and the surface ($\Delta fCO_2$) were quite
647 similar considering both the dolomite buffer and carbonate/alumino-silicate buffer for the
648 thermal waters in the Granada Basin. A mineral assemblage buffering at depth mainly
649 composed of carbonates, evaporites, and quartz characterizes this system.

650 The group of waters located in the graben in the Alpujárride Complex presents the lowest
651 reservoir temperature of 55-60°C and $fCO_2$ ranging from $5 \times 10^{-3}$ to $7 \times 10^{-2}$, depending of the
652 considered buffering minerals. The $\Delta fCO_2$ between the depth and the surface is higher with the
653 dolomite buffer than with the carbonate and alumino-silicate buffer. The buffering mineral
654 assemblage at depth is estimated to be carbonates, quartz, and Ca alumino-silicates.

655 On the other hand, the group of waters located at contact with metamorphic complexes
656 shows the highest reservoir temperature of 130 – 140°C and $fCO_2$ ranging from approximatively
657 1 to 100. The $\Delta fCO_2$ between the depth and the surface is lower with the dolomite buffer than
658 with the carbonate and alumino-silicate buffer. The buffering mineral assemblage in the
659 reservoir might be dolomite, quartz, Mg and Ca alumino-silicates.

660 This study highlights the importance of evaluating the mineral buffers in the reservoir
661 conditions of the geothermal systems. The mineral assemblage at equilibrium in the reservoir
662 conditions constrains the estimated $CO_2$ generation and release at depth. In the case study of
663 the Central Betic Cordillera, $CO_2$ degassing is more constrained in the evaporitic basins thanks
664 to a strong carbonate/evaporite/quartz buffer than in the surrounding areas of the basins where
665 the alumino-silicates play a non-negligible role. Moreover, we pointed out the key role of the
666 reservoir temperature on the estimation of the reactions between $CO_2$, water, and rocks for the
667 geothermal systems in sedimentary basins.

668 The estimations of $CO_2$ emissions generated by the thermal systems for potential
669 household heating purpose indicate that the geothermal energy is globally a clean energy but
670 might release as much $CO_2$ as a natural gas furnace for the thermal waters with the highest
671 reservoir temperature. This study points out the importance to estimate properly the amount of
672 $CO_2$ degassing in geothermal waters depending of the reservoir conditions. Our results
673 highlight the importance of considering geochemical estimates for heat exchanger design. In
674 the case of thermal waters with the highest temperatures and high $CO_2$ contents, heat
675 exchangers allowing to maintain fluids under pressure might be preferred to avoid $CO_2$ release
676 in the atmosphere.
677

**Acknowledgments:**

The Authors thank N. Labourdette and E. Aubry for their help in water analyses and Claudio Inguaggiato for helping collecting gas samples during the sampling survey. The Authors are also grateful to M. Rouelle, M. Azaroual, and P. Sarda for the fruitful discussions during various stages of this study. The Authors thank the two Reviewers for their fruitful comments that helped to improve the quality and the clarity of the manuscript. This work was supported by IFPEN and Sorbonne Université. We also thank the Istituto Nazionale di Geofisica e Vulcanologia – Palermo (INGV) for gas analyses.

**References:**


Ármannsson, H., 2018. An overview of carbon dioxide emissions from Icelandic geothermal areas. Appl. Geochemistry 97, 11–18. https://doi.org/10.1016/j.apgeochem.2018.07.013

Ármannsson, H., 2003. CO2 emission from geothermal plants, in: International Geothermal Conference. pp. 56–62.

Arnórsson, S., Gunnlaugsson, E., Svavarsson, H., 1983. The chemistry of geothermal waters in Iceland. III. Chemical geothermometry in geothermal investigations. Geochim. Cosmochim. Acta 47, 567–577. https://doi.org/10.1016/0016-7037(83)90278-8

Arrizabalaga, I., De Gregorio, M., García del la Noceda, C., Hidalgo, R., Urchueguía, J.F., 2015. Country Update for the Spanish Geothermal Sector, in: World Geothermal Congress 2015. p. 9.

Asta, M.P., Gimeno, M.J., Auqué, L.F., Gómez, J., Acero, P., Lapuente, P., 2012. Hydrochemistry and geothermometrical modeling of low-temperature Panticosa geothermal system (Spain). J. Volcanol. Geotherm. Res. 235–236, 84–95. https://doi.org/10.1016/j.jvolgeores.2012.05.007

Auqué, L.F., Acero, P., Gimeno, M.J., Gómez, J.B., Asta, M.P., 2009. Hydrogeochemical modeling of a thermal system and lessons learned for CO2 geologic storage. Chem. Geol. 268, 324–336. https://doi.org/10.1016/j.chemgeo.2009.09.011

Azañón, J.M., Crespo-Blanc, A., 2000. Exhumation during a continental collision inferred from the tectonometamorphic evolution of the Alpujarride Complex in the central Betics (Alboran Domain, SE Spain). Tectonics 19, 549–565. https://doi.org/10.1029/2000TC900005

Azañón, J.M., García-Dueñas, V., Goffé, B., 1998. Exhumation of high-pressure metapelites and coeval crustal extension in the Alpujarride complex (Betic Cordillera). Tectonophysics 285, 231–252. https://doi.org/10.1016/S0040-1951(97)00273-4

Battistel, M., Hurwitz, S., Evans, W.C., Barbieri, M., 2016. The chemistry and isotopic composition of waters in the low-enthalpy geothermal system of Cimino-Vico Volcanic District, Italy. J. Volcanol. Geotherm. Res. 328, 222–229. https://doi.org/10.1016/j.jvolgeores.2016.11.005

Benavente Herrera, J., Sanz de Galdeano, C., 1985. Relacion de las direcciones de karstificacion y del termalismo con la fracturacion en las Cordilleras Beticas. Estud. Geológicos 41, 177–188.

Bjorlykke, K., Egeberg, P.K., 1993. Quartz cementation in sedimentary basins. Am. Assoc. Pet. Geol. Bull. 77, 1538–1548.

720 Blasco, M., Auqué, L.F., Gimeno, M.J., Acero, P., Asta, M.P., 2017. Geochemistry,
721 geothermometry and influence of the concentration of mobile elements in the chemical
722 characteristics of carbonate-evaporitic thermal systems. The case of the Tiermas
723 geothermal system (Spain). Chem. Geol. 466, 696–709.
724 https://doi.org/10.1016/J.CHEMGEO.2017.07.013
725 Blasco, M., Gimeno, M.J., Auqué, L.F., 2018. Low temperature geothermal systems in
726 carbonate-evaporitic rocks: Mineral equilibria assumptions and geothermometrical
727 calculations. Insights from the Arnedillo thermal waters (Spain). Sci. Total Environ. 615,
728 526–539. https://doi.org/10.1016/J.SCITOTENV.2017.09.269
729 Braga, J.C., Martín, J.M., Quesada, C., 2003. Patterns and average rates of late Neogene--
730 Recent uplift of the Betic Cordillera, SE Spain. Geomorphology 50, 3–26.
731 https://doi.org/10.1016/S0169-555X(02)00205-2
732 Buforn, E., Bezzeghoud, M., Udías, A., Pro, C., 2004. Seismic Sources on the Iberia-African
733 Plate Boundary and their Tectonic Implications. Pure Appl. Geophys. 161, 623–646.
734 https://doi.org/10.1007/s00024-003-2466-1
735 Campos, J.C.R., 2006. Guía de manantiales de la provincia de Granada: Una visión sobre su
736 origen y naturaleza. Publicaciones de Diputación Provincial de Granada.
737 Capasso, G., Favara, R., Grassa, F., Inguaggiato, S., Longo, M., 2005. On-line technique for
738 preparing and measuring stable carbon isotope of total dissolved inorganic carbon in water
739 samples ($\delta^{13}$CTDIC). Ann. Geophys. 48, 159–166.
740 Capasso, G., Inguaggiato, S., 1998. A simple method for the determination of dissolved gases
741 in natural waters. An application to thermal waters from Vulcano Island. Appl.
742 Geochemistry 13, 631–642. https://doi.org/10.1016/S0883-2927(97)00109-1
743 Capecchiacci, F., Tassi, F., Vaselli, O., Bicocchi, G., Cabassi, J., Giannini, L., Nisi, B.,
744 Chiocciora, G., 2015. A combined geochemical and isotopic study of the fluids discharged
745 from the Montecatini thermal system (NW Tuscany, Italy). Appl. Geochemistry 59, 33–
746 46. https://doi.org/10.1016/j.apgeochem.2015.03.010
747 Centre d'Expertise en Analyse Environnementale du Québec, 2016. Détermination de la silice
748 réactive dans l'eau : méthode par spectrophotométrie UV-visible, MA. 303 – SiO2 1.0,
749 rév. 1. Ministère du Développement durable, de l'Environnement, de la Lutte contre les
750 changements climatiques.
751 Cerón, J.C., López-Chicano, M., 2002. Thermal waters in Andalucía. Newsl. Int. Geotherm.
752 Assoc. 48, 4–5.
753 Chiodini, G., Baldini, A., Barberi, F., Carapezza, M.L., Cardellini, C., Frondini, F., Granieri,

754 D., Ranaldi, M., 2007. Carbon dioxide degassing at Latera caldera (Italy): Evidence of
755 geothermal reservoir and evaluation of its potential energy. J. Geophys. Res. 112, 1–17.
756 https://doi.org/10.1029/2006JB004896
757 Chiodini, G., Cioni, R., Guidi, M., Raco, B., Marini, L., 1998. Soil $CO_2$ flux measurements in
758 volcanic and geothermal areas. Appl. Geochemistry 13, 543–552.
759 Chiodini, G., Frondini, F., Marini, L., 1995a. Theoretical geothermometers and $PCO_2$ indicators
760 for aqueous solutions coming from hydrothermal systems of medium-low temperature
761 hosted in carbonate-evaporite rocks. Application to the thermal springs of the Etruscan
762 Swell, Italy. Appl. Geochemistry 10, 337–346. https://doi.org/10.1016/0883-
763 2927(95)00006-6
764 Chiodini, G., Frondini, F., Ponziani, F., 1995b. Deep structures and carbon dioxide degassing
765 in Central Italy. Geothermics 24, 81–94. https://doi.org/10.1016/0375-6505(94)00023-6
766 Clark, I.D., Fritz, P., 1997. Environmental isotopes in hydrogeology. CRC Press/Lewis
767 Publishers, Boca Raton, FL.
768 Corbí, H., Lancis, C., García-García, F., Pina, J.-A., Soria, J.M., Tent-Manclús, J.E., Viseras,
769 C., 2012. Updating the marine biostratigraphy of the Granada Basin (central Betic
770 Cordillera). Insight for the Late Miocene palaeogeographic evolution of the Atlantic --
771 Mediterranean seaway. Geobios 45, 249–263.
772 https://doi.org/10.1016/j.geobios.2011.10.006
773 Coudrain-Ribstein, A., Gouze, P., de Marsily, G., 1998. Temperature-carbon dioxide partial
774 pressure trends in confined aquifers. Chem. Geol. 1, 73–89.
775 https://doi.org/https://doi.org/10.1016/S0009-2541(97)00161-7
776 Cruz-Sanjulián, J., Rossell, L.G., Blasco, J.G., 1972. Aguas termales de la provincia de
777 Granada. Bol. Geológico y Min. T.LXXXIII-III 266–275.
778 Cruz Sanjulián, J., Granda, J.M., 1979. Temperatura de base de las aguas termales de la
779 provincia de Granada, in: II Simposio Nacional de Hidrogeología. pp. 547–568.
780 D'Amore, F., Arnórsson, S., Geothermometry, S.A., 2000. Isotopic and Chemical Techniques
781 in Geothermal Exploration. Dev. Use Sampl. Methods, Data Handl. Interpret. Int. At.
782 Energy Agency, Vienna, Austria 152–199.
783 D'Amore, F., Fancelli, R., Caboi, R., 1987. Observations on the application of chemical
784 geothermometers to some hydrothermal systems in Sardinia. Geothermics 16, 271–282.
785 Elidemir, S., Güleç, N., 2018. Geochemical characterization of geothermal systems in western
786 Anatolia (Turkey): implications for CO2trapping mechanisms in prospective CO2-EGS
787 sites. Greenh. Gases Sci. Technol. 8, 63–76. https://doi.org/10.1002/ghg.1747

788 Fernàndez, M., Marzán, I., Correia, A., Ramalho, E., 1998. Heat flow, heat production, and
789 lithospheric thermal regime in the Iberian Peninsula. Tectonophysics 291, 29–53.
790 https://doi.org/10.1016/s0040-1951(98)00029-8
791 Fournier, R.O., 1977. Chemical geothermometers and mixing models for geothermal systems.
792 Geothermics 5, 41–50. https://doi.org/10.1016/0375-6505(77)90007-4
793 Fournier, R.O., Potter, R.W., 1982. An equation correlating the solubility of quartz in water
794 from 25° to 900°C at pressures up to 10,000 bars. Geochim. Cosmochim. Acta 46, 1969–
795 1973. https://doi.org/10.1016/0016-7037(82)90135-1
796 Fusari, A., Carroll, M.R., Ferraro, S., Giovannetti, R., Giudetti, G., Invernizzi, C., Mussi, M.,
797 Pennisi, M., 2017. Circulation path of thermal waters within the Laga foredeep basin
798 inferred from chemical and isotopic (δ18O, δD, 3H, 87Sr/86Sr) data. Appl. Geochemistry
799 78, 23–34. https://doi.org/10.1016/J.APGEOCHEM.2016.11.021
800 Galindo-Zaldívar, J., Gil, A.J., Sanz de Galdeano, C., Lacy, M.C., García-Armenteros, J.A.,
801 Ruano, P., Ruiz, A.M., Martínez-Martos, M., Alfaro, P., 2015. Active shallow extension
802 in central and eastern Betic Cordillera from CGPS data. Tectonophysics 663, 290–301.
803 https://doi.org/10.1016/j.tecto.2015.08.035
804 Gran, G., 1952. Determination of the equivalence point in potentiometric titrations. Part II.
805 Analyst 77, 661–671. https://doi.org/10.1039/AN9527700661
806 Harvey, M.C., Rowland, J. V, Chiodini, G., Rissmann, C.F., Bloomberg, S., Fridriksson, T.,
807 Oladottir, A.A., 2017. $CO_2$ flux geothermometer for geothermal exploration. Geochim.
808 Cosmochim. Acta 213, 1–16. https://doi.org/10.1016/j.gca.2017.06.025
809 Hunt, T.M., 2001. Five Lectures on Environmental Effects of Geothermal Utilization,
810 Geothermal Training Programme.
811 Hutcheon, I.A.N., Shevalier, M., Abercrombie, H.J., 1993. pH buffering by metastable mineral-
812 fluid equilibria and evolution of carbon dioxide fugacity during burial diagenesis.
813 Geochim. Cosmochim. Acta 57, 1017–1027.
814 Inguaggiato, S., Rizzo, A., 2004. Dissolved helium isotope ratios in ground-waters: a new
815 technique based on gas--water re-equilibration and its application to Stromboli volcanic
816 system. Appl. Geochemistry 19, 665–673.
817 https://doi.org/10.1016/j.apgeochem.2003.10.009
818 Lapillonne, B., Pollier, K., Samci, N., 2014. Energy efficiency trends for households in the EU.
819 Enerdata. Retrieved June 22, 2015.
820 Lix, C., Zuddas, P., Inguaggiato, C., Guichet, X., Benavente, J., Barbier, M., 2018. New insights
821 on Betic Cordillera structure from gas geochemistry. Geochemistry, Geophys. Geosystems

822 1–12. https://doi.org/10.1029/2018GC007712
823 López-Chicano, M., Bouamama, M., Vallejos, A., Pulido-Bosch, A., 2001a. Factors which
824 determine the hydrogeochemical behaviour of karstic springs. A case study from the Betic
825 Cordilleras, Spain. Appl. Geochemistry 16, 1179–1192. https://doi.org/10.1016/S0883-
826 2927(01)00012-9
827 López-Chicano, M., Cerón, J.C., Vallejos, A., Pulido-Bosch, A., 2001b. Geochemistry of
828 thermal springs, Alhama de Granada (southern Spain). Appl. Geochemistry 16, 1153–
829 1163. https://doi.org/10.1016/S0883-2927(01)00020-8
830 Marini, L., Chiodini, G., Cioni, R., 1986. New geothermometers for carbonate-evaporite
831 geothermal reservoirs. Geothermics 15, 77–86. https://doi.org/10.1016/0375-
832 6505(86)90030-1
833 Martín-Algarra, A., Martín-Martín, M., Andreo, B., Julià, R., González-Gómez, C., 2003.
834 Sedimentary patterns in perched spring travertines near Granada (Spain) as indicators of
835 the paleohydrological and paleoclimatological evolution of a karst massif. Sediment. Geol.
836 161, 217–228. https://doi.org/10.1016/S0037-0738(03)00115-5
837 Martín, J.M., Braga, J.C., 1987. Alpujárride carbonate deposits (southern Spain) - Marine
838 Sedimentation in a Triassic Atlantic. Palaeogeogr. Palaeoclimatol. Palaeoecol. 59, 243–
839 260.
840 McCay, A.T., Feliks, M.E.J., Roberts, J.J., 2019. Life cycle assessment of the carbon intensity
841 of deep geothermal heat systems: A case study from Scotland. Sci. Total Environ. 685,
842 208–219. https://doi.org/10.1016/j.scitotenv.2019.05.311
843 Michard, G., 1990. Behaviour of major elements and some trace elements (Li, Rb, Cs, Sr, Fe,
844 Mn, W, F) in deep hot waters from granitic areas. Chem. Geol. 89, 117–134.
845 https://doi.org/10.1016/0009-2541(90)90062-C
846 Michard, G., 1979. Géothermomètres chimiques. Bull. BRGM 2, 183–189.
847 Parkhurst, D.L., Appelo, C.A.J., others, 2013. Description of input and examples for
848 PHREEQC version 3 - a computer program for speciation, batch-reaction, one-
849 dimensional transport, and inverse geochemical calculations. US Geol. Surv. Tech.
850 methods, B. 6, 497. https://doi.org/10.1016/0029-6554(94)90020-5
851 Pérez del Villar, L., 2009. Almacenamiento geológico de CO2: Análogos del almacenamiento
852 y escape. Fundamentos, ejemplos y aplicaciones para la predicción de riesgos y la
853 evaluación del comportamiento a largo plazo. Congr. Nac. del Medio Ambient.
854 Prado-Pérez, A.J., Pérez del Villar, L., 2011. Dedolomitization as an analogue process for
855 assessing the long-term behaviour of a CO2 deep geological storage: The Alicún de las

Torres thermal system (Betic Cordillera, Spain). Chem. Geol. 289, 98–113. https://doi.org/10.1016/j.chemgeo.2011.07.017

Rimstidt, J.D., Barnes, H.L., 1980. The kinetics of silica-water reactions. Geochim. Cosmochim. Acta 44.

Rodríguez-Fernández, J., Sanz de Galdeano, C., 2006. Late orogenic intramontane basin development : the Granada basin, Betics (southern Spain). Basin Res. 18, 85–102. https://doi.org/10.1111/j.1365-2117.2006.00284.x

Sánchez Guzmán, J., García de la Noceda, C., 2010. The Evolution of Geothermal Energy in Spain - Country Update (2005-2009), in: Proceedings World Geothermal Congress.

Sanz de Galdeano, C., 2008. The Cadiz-Alicante fault: an important discontinuity in the Betic Cordillera. Rev. la Soc. Geológica España 21.

Sanz de Galdeano, C., 1990. Geologic evolution of the Betic Cordilleras in the Western Mediterranean, Miocene to the present. Tectonophysics 172, 107–119. https://doi.org/10.1016/0040-1951(90)90062-D

Sanz de Galdeano, C., Peláez, J.A., 2011. Fallas activas en la Cordillera Bética: una aproximación a partir de la información tectónica y sísmica. Editorial Universidad de Granada.

Sanz de Galdeano, C., Peláez, J.A., 2011. Fallas activas en la Cordillera Bética : una aproximación a partir de la información tectónica y sísmica.

Sanz de Galdeano, C., Vera, J.A., 1992. Stratigraphic record and palaeogeographical context of the Neogene basins in the Betic Cordillera, Spain. Basin Res. 4, 21–36. https://doi.org/10.1111/j.1365-2117.1992.tb00040.x

Seward, T.M., Kerrick, D.M., 1996. Hydrothermal $CO_2$ emission from the Taupo volcanic zone, New Zealand. Earth Planet. Sci. Lett. 139, 105–113.

Tole, M.P., Ármannsson, H., Zhong-He, P., Arnórsson, S., 1993. Fluid/mineral equilibrium calculations for geothermal fluids and chemical geothermometry. Geothermics 22, 17–37.

Verma, M.P., 2000a. Chemical thermodynamics of silica: A critique on its geothermometer. Geothermics 29, 323–346. https://doi.org/10.1016/S0375-6505(99)00064-4

Verma, M.P., 2000b. Limitations in applying silica geothermometers for geothermal reservoir evaluation, in: Proceedings, 25th Workshop on Geothermal Reservoir Engineering, Stanford University, Stanford. pp. 24–26.

889 *List of the figures:*



922

923 Figure 1

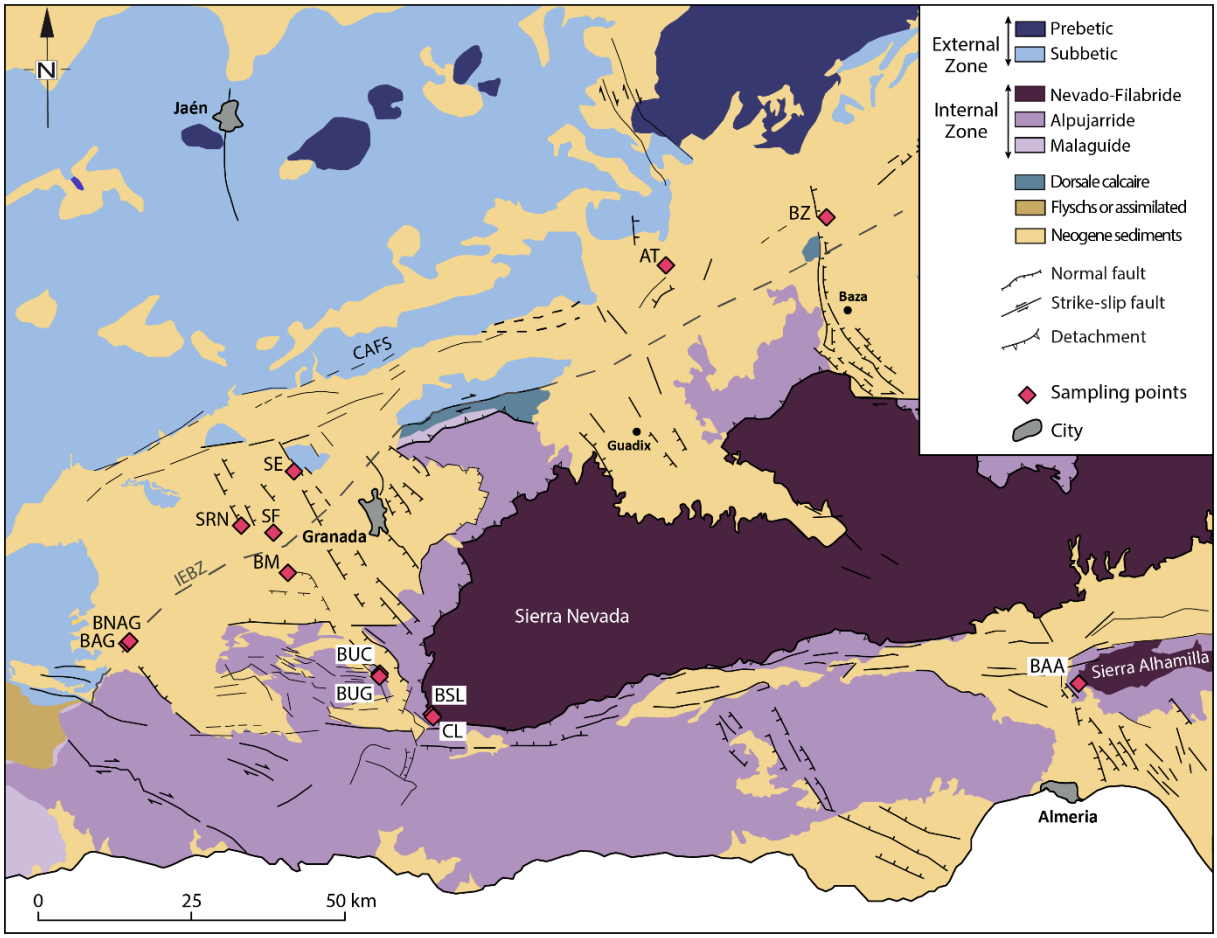


924

925

926 Figure 2

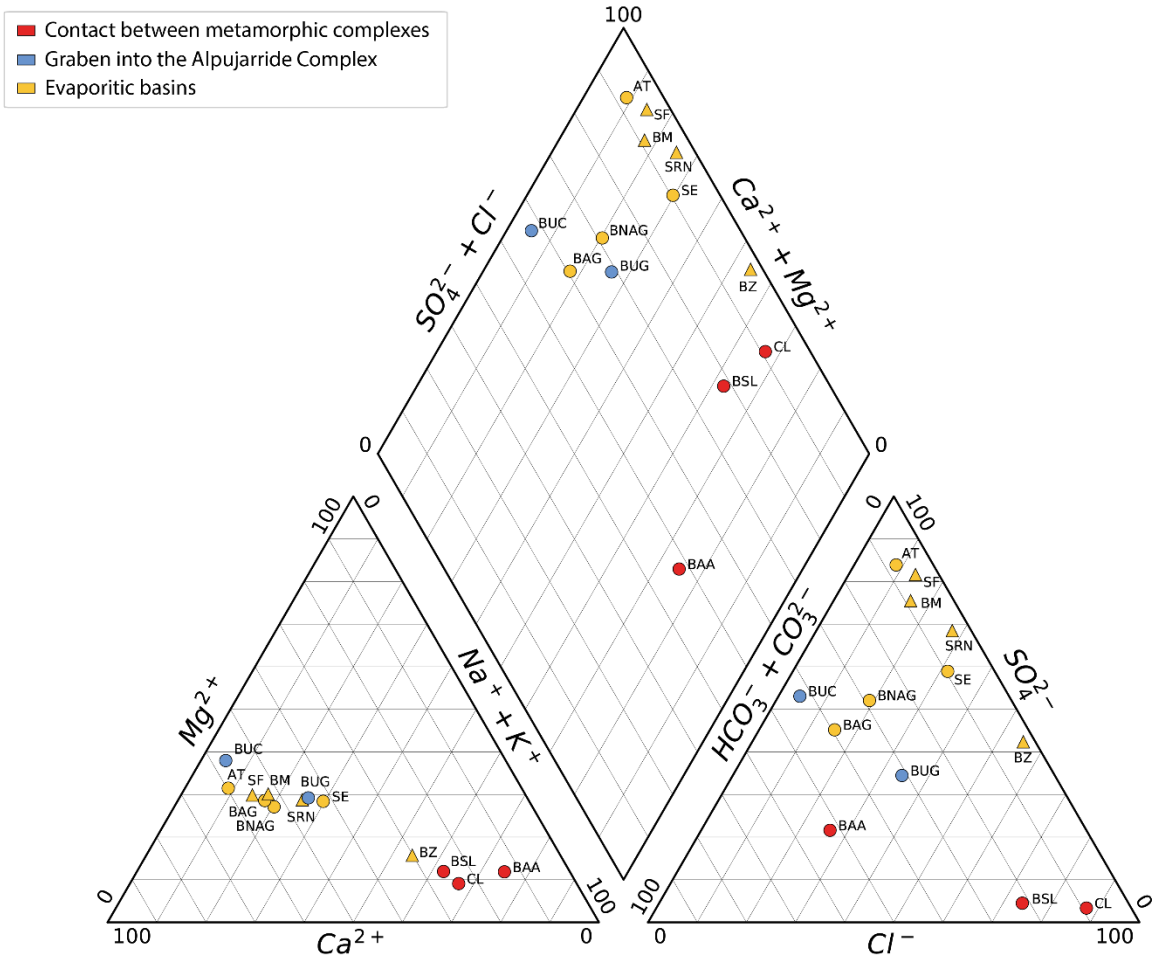


927

928

929 Figure 3

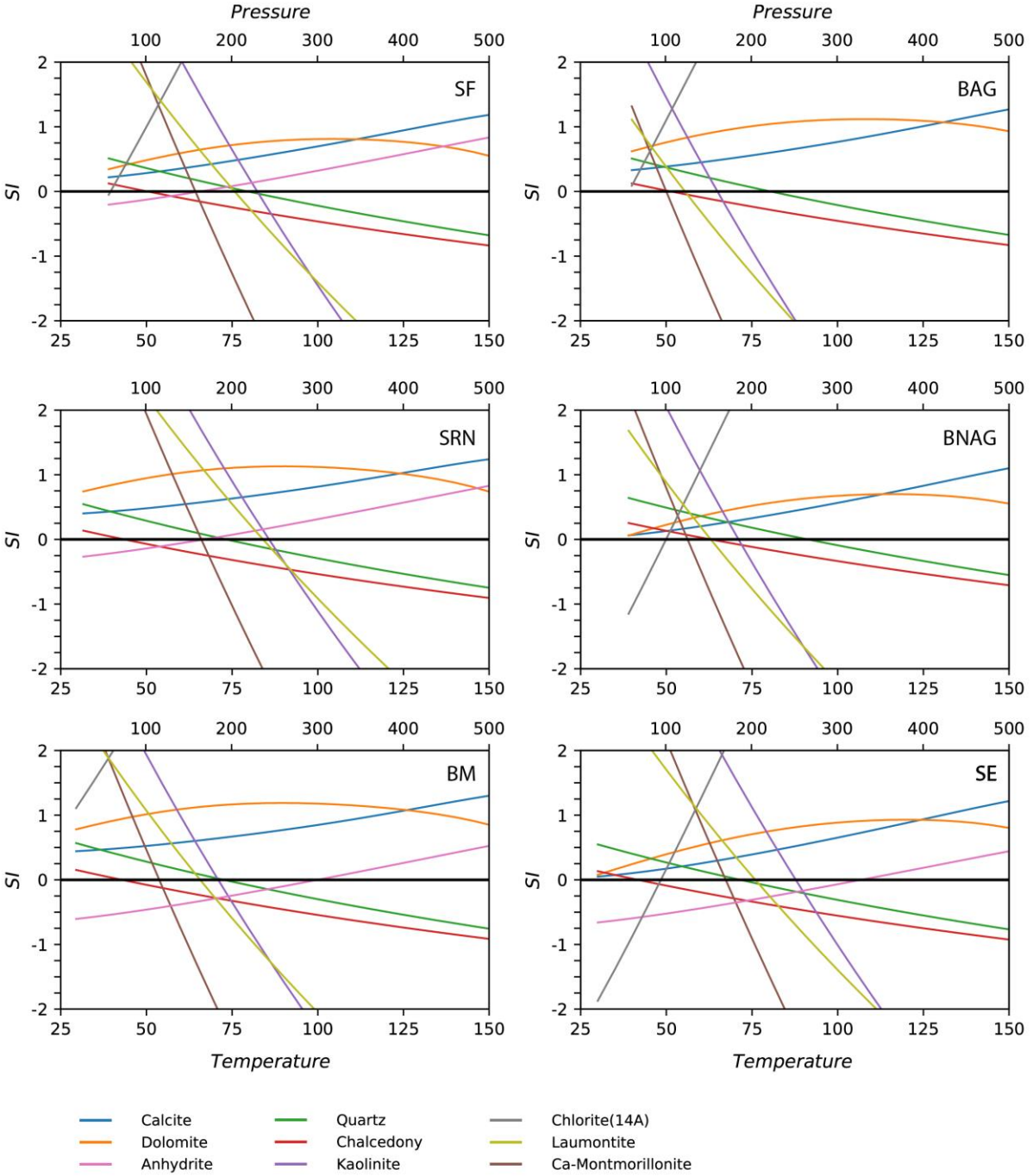


930

931

932 Figure 4

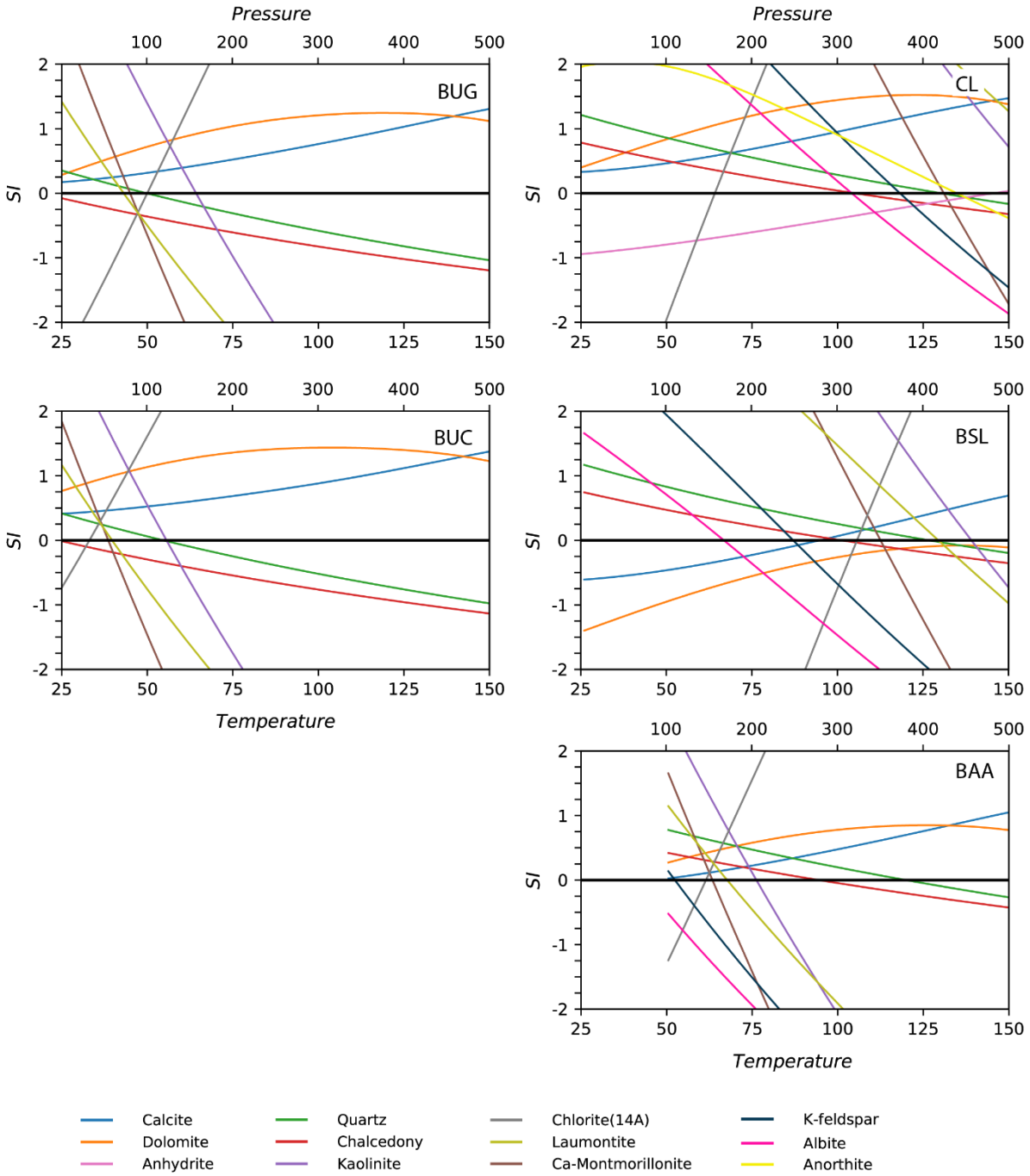


933

934

935 Figure 5

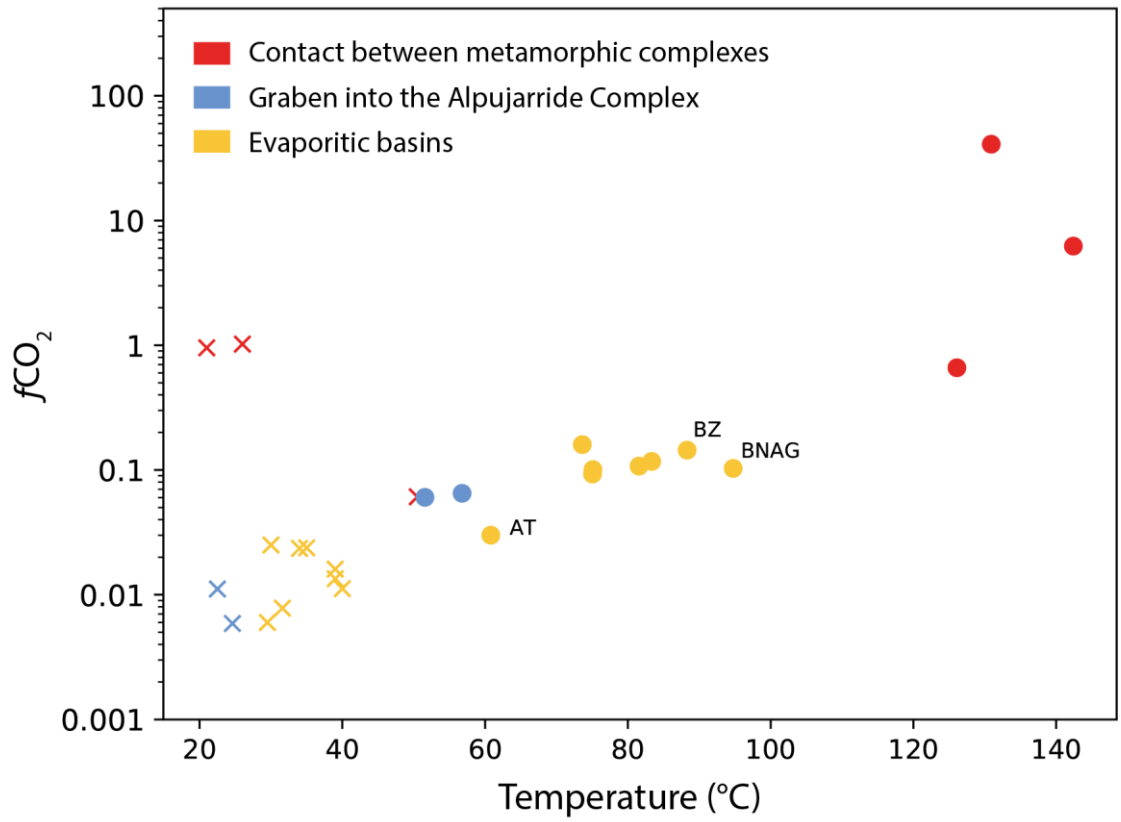


936

937

938 Figure 6

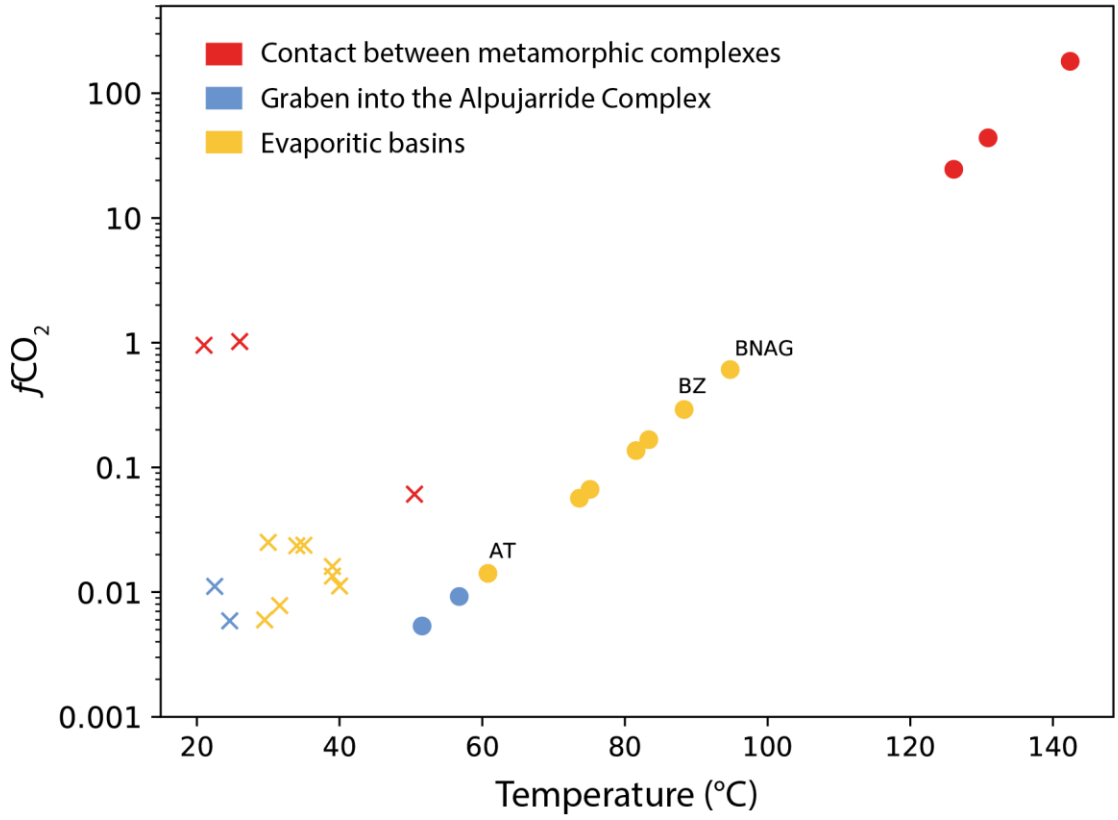


939

940

941 Figure 7

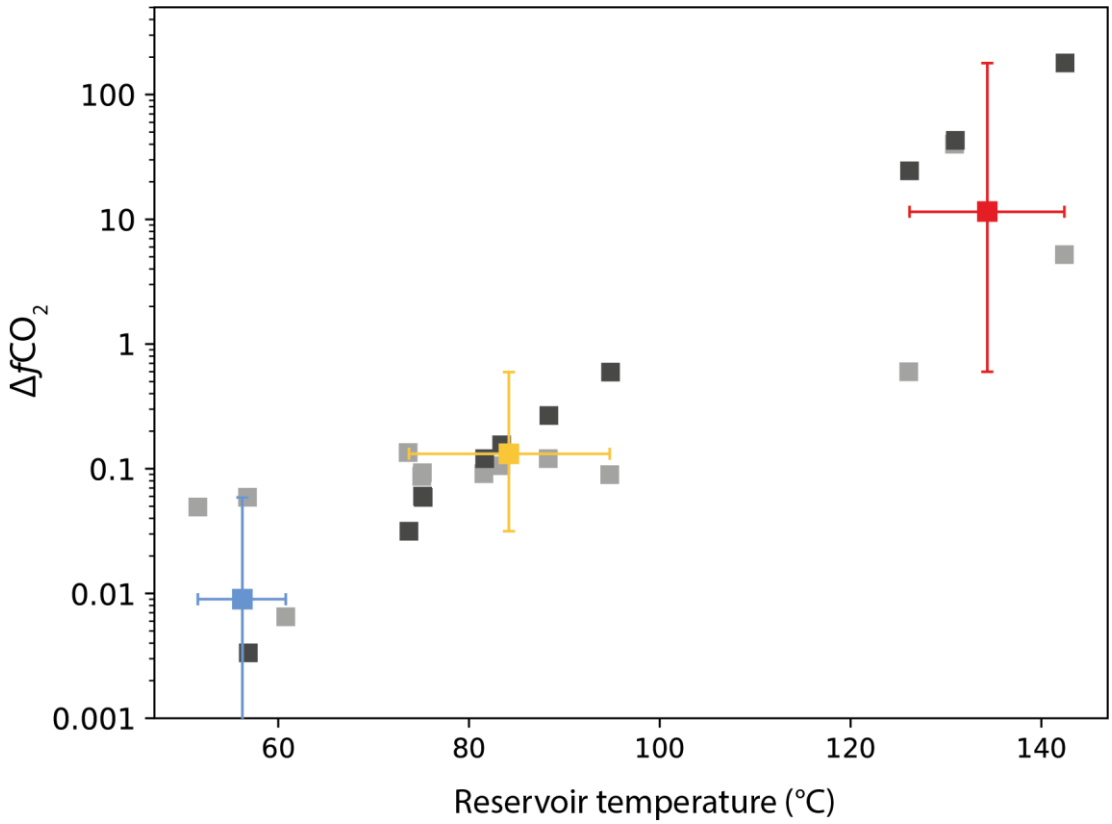


942

943

944 Figure 8

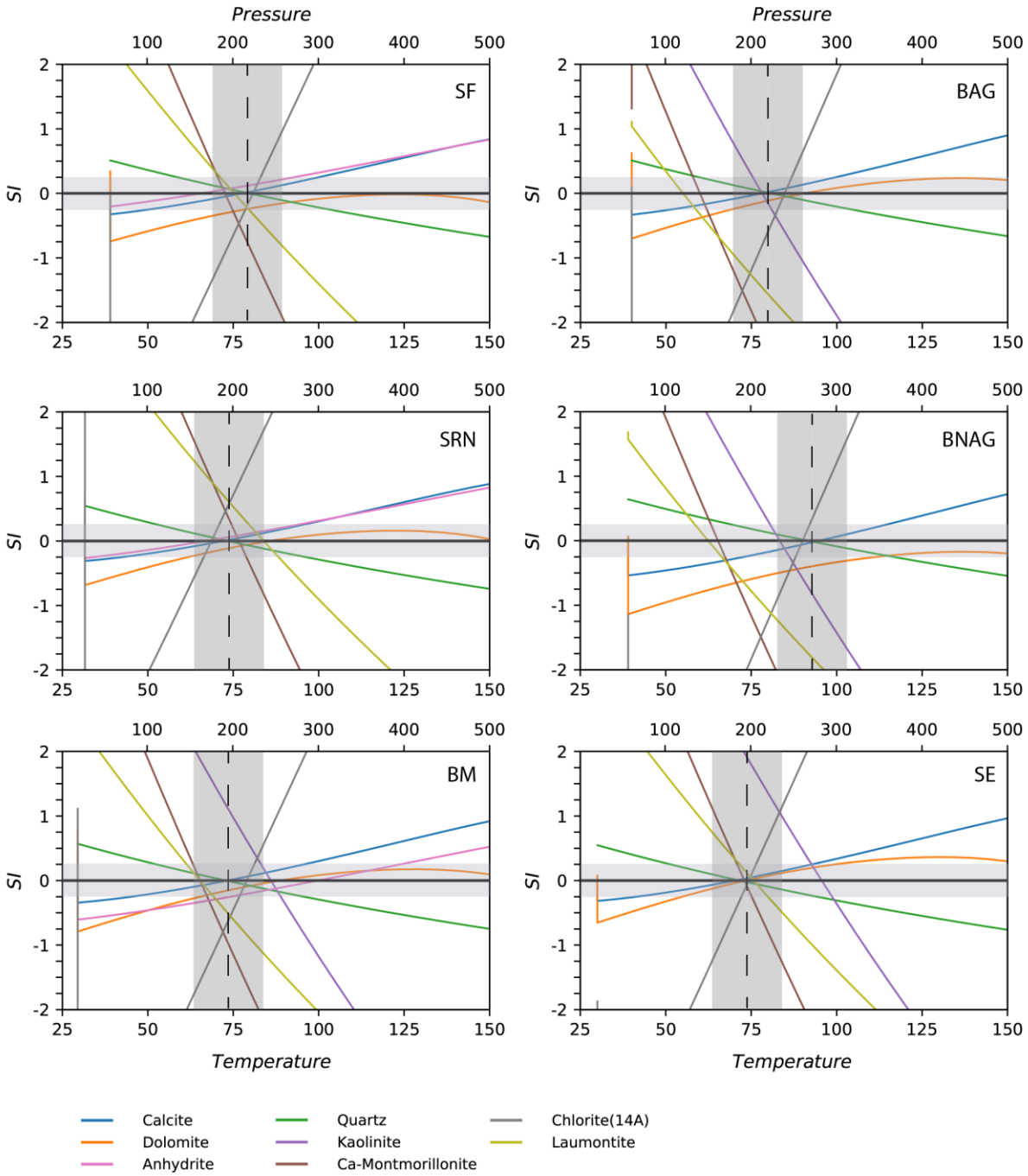


945

946

947 Figure 9

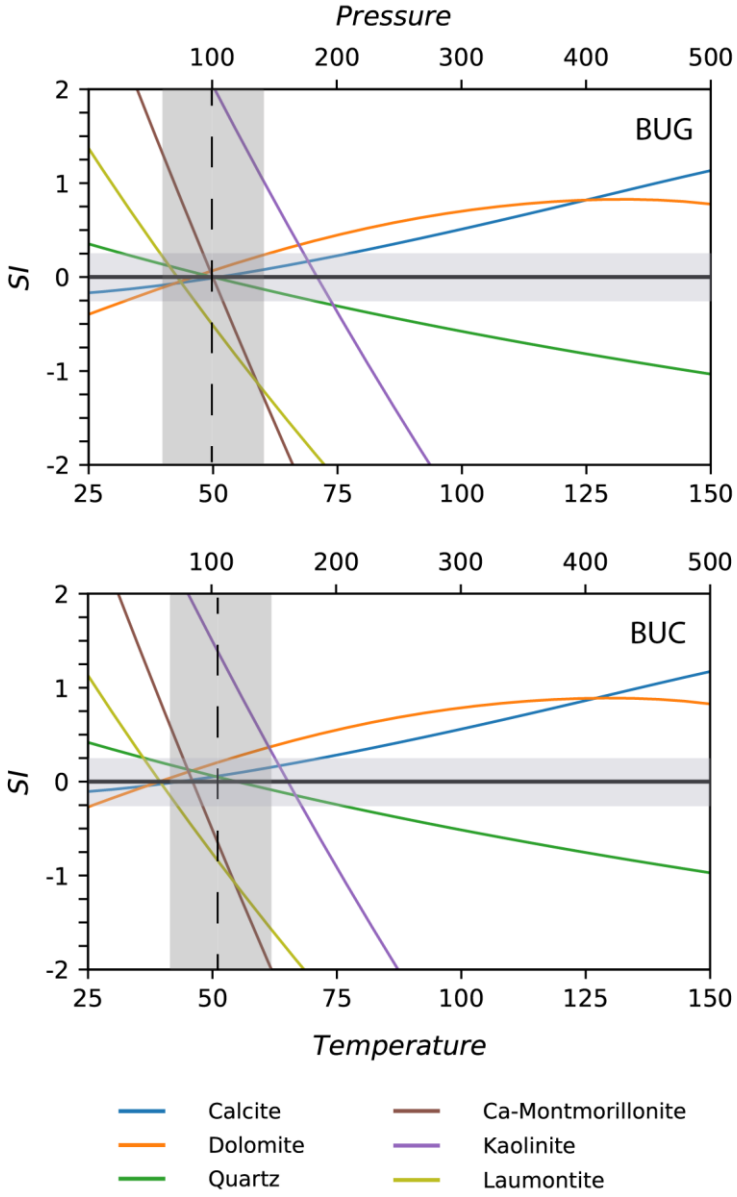


948

949

950 Figure 10

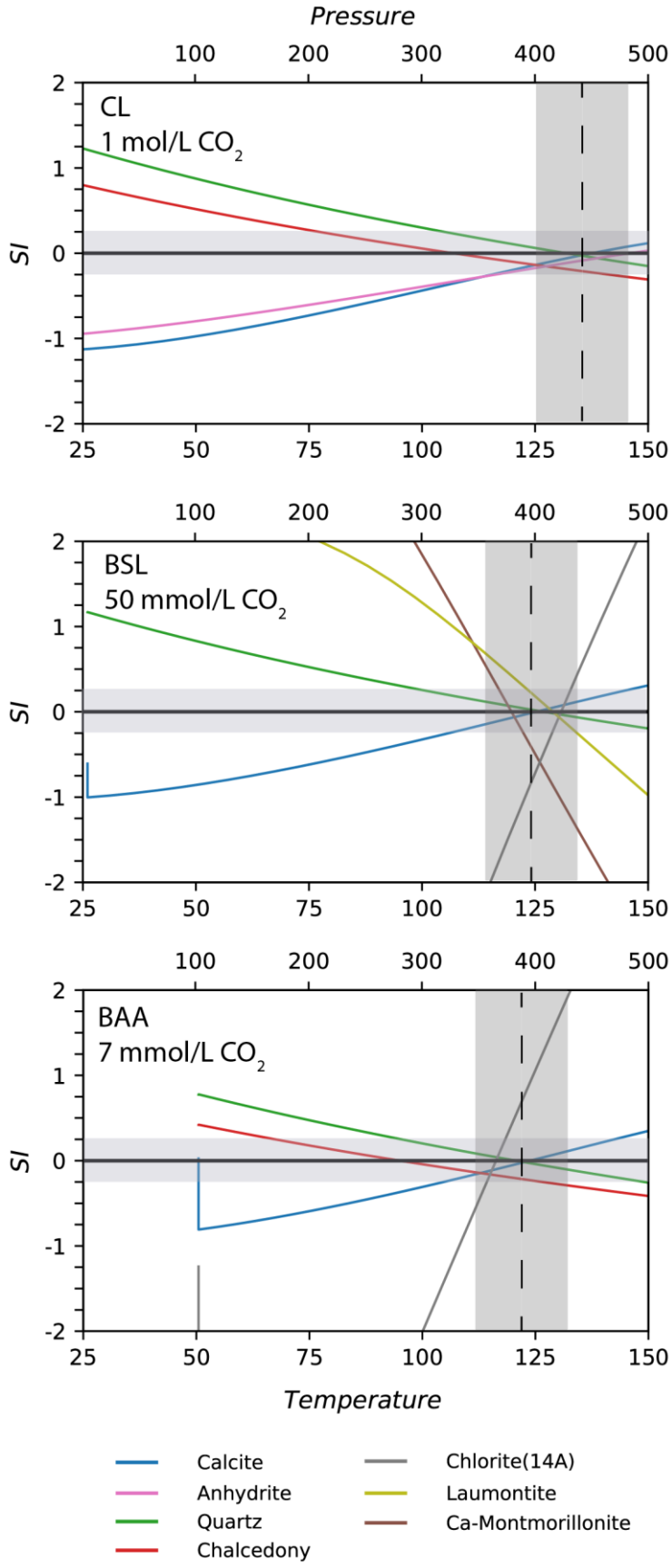


951

952

953 Figure 11

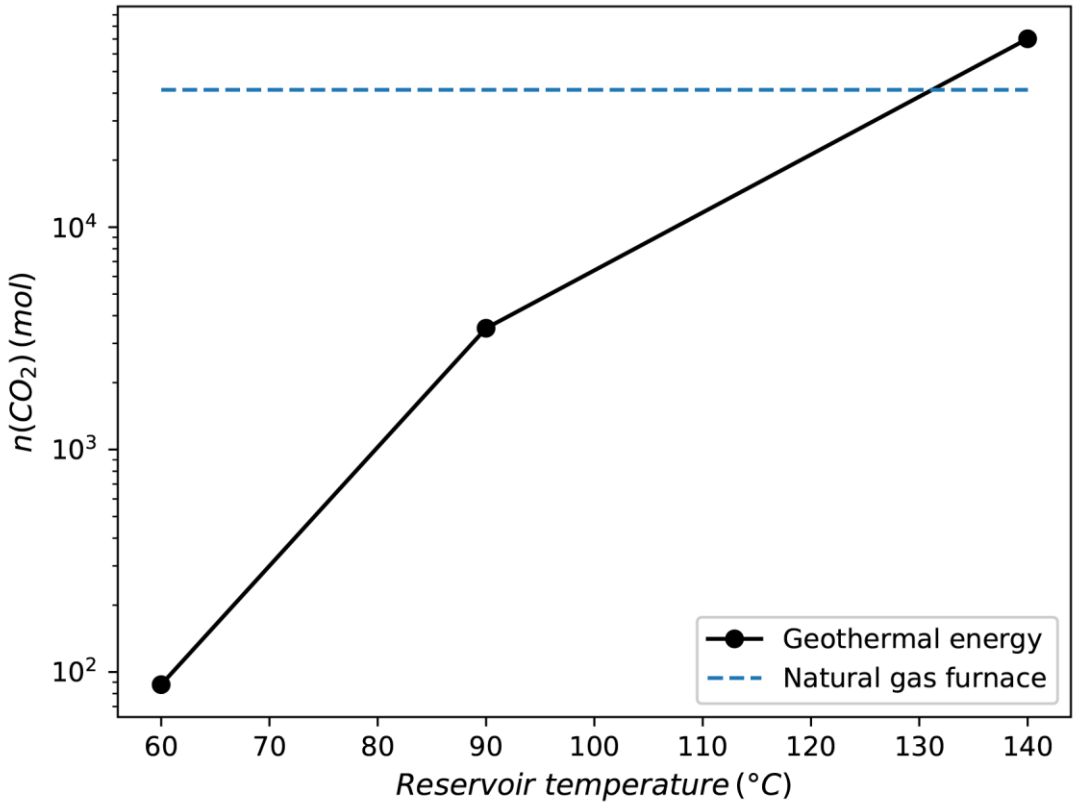


954

| Sample and location | Code | Type | Depth (m) | Temp. (°C) | pH | EC | Ca | Mg | Na | K | Alk. | Cl | $SO_4$ | Si | Al | Ba | Fe | Sr | TDS | CBE |
|---|---|---|---|---|---|---|---|---|---|---|---|---|---|---|---|---|---|---|---|---|
| ***Contacts metamorphic complexes*** | | | | | | | | | | | | | | | | | | | | |
| Banos Salado de Lanjaron | BSL | S | | 26 | 5.8 | 8.18 | 6.59 | 3.06 | 29.5 | 2.60 | 12.9 | 44.0 | 1.31 | 1.56 | 8.85E-03 | 1.04E-03 | 3.13E-01 | 0.19 | 3.72 | 7.29 |
| 36°55.4189'N; 3°29.5869'W | | | | | | | | | | | | | | | | | | | | |
| Capuchina de Lanjaron | CL | S | | 21 | 6.1 | 34.15 | 32.6 | 12.3 | 167 | 14.0 | 28.7 | 275 | 5.24 | 1.53 | 7.13E-02 | 7.34E-04 | 4.98E-01 | 0.62 | 18.17 | 7.40 |
| 36°55.1523'N, 3°29.4182'W | | | | | | | | | | | | | | | | | | | | |
| Banos de Alhamilla | BAA | S | | 51 | 7.1 | 1.92 | 0.88 | 0.78 | 9.65 | 0.23 | 7.93 | 3.99 | 1.64 | 1.38 | 4.92E-04 | 4.62E-04 | 9.66E-04 | 0.02 | 1.15 | 7.04 |
| 36°57.6531'N; 2°23.7875'W | | | | | | | | | | | | | | | | | | | | |
| ***Graben into Alp. Complex*** | | | | | | | | | | | | | | | | | | | | |
| Banos Urquizar Chico | BUC | S | | 25 | 7.6 | 0.99 | 2.62 | 1.75 | 0.42 | 0.05 | 3.99 | 0.41 | 2.49 | 0.27 | 6.99E-04 | 2.28E-04 | b.d.l | 0.05 | 0.68 | 0.87 |
| 36°58.3477'N; 3°34.5347'W | | | | | | | | | | | | | | | | | | | | |
| Banos Urquizar Grande | BUG | S | | 23 | 7.3 | 1.50 | 2.92 | 1.92 | 3.22 | 0.22 | 4.21 | 4.66 | 2.33 | 0.24 | 1.23E-03 | 2.33E-04 | b.d.l | 0.04 | 0.91 | 1.49 |
| 36°58.2261'N; 3°34.5854'W | | | | | | | | | | | | | | | | | | | | |
| ***Evaporitic basin*** | | | | | | | | | | | | | | | | | | | | |
| Banos de la Malaha | BM | W | 200 | 30 | 7.4 | 3.08 | 8.05 | 4.59 | 5.25 | 0.22 | 2.89 | 5.10 | 12.1 | 0.45 | 1.60E-03 | 1.18E-04 | 2.98E-02 | 0.16 | 2.13 | 2.35 |
| 37°06.2946'N, 3°43.6034'W | | | | | | | | | | | | | | | | | | | | |
| Santa Fe | SF | W | 510 | 39 | 7.0 | 4.69 | 13.7 | 7.30 | 6.82 | 0.34 | 2.58 | 7.15 | 21.1 | 0.53 | 2.09E-03 | 5.10E-05 | 6.50E-03 | 0.16 | 3.38 | 2.73 |
| 37°09.3813'N; 3°45.2023'W | | | | | | | | | | | | | | | | | | | | |
| Sondeo Romilla la Nueva | SRN | W | 740 | 32 | 7.3 | 6.13 | 14.3 | 8.80 | 15.5 | 0.41 | 2.72 | 18.9 | 23.2 | 0.45 | 5.13E-03 | 8.92E-05 | 4.25E-02 | 0.17 | 4.26 | 4.48 |
| 37°10.0216'N; 3°48.8567'W | | | | | | | | | | | | | | | | | | | | |
| Sierra Elvira | SE | S | | 30 | 6.9 | 3.82 | 7.80 | 5.28 | 10.8 | 0.27 | 3.77 | 12.4 | 11.6 | 0.43 | 3.74E-03 | 1.35E-04 | b.d.l | 0.11 | 2.52 | 2.93 |
| 37°13.7033'N; 3°43.3372'W | | | | | | | | | | | | | | | | | | | | |
| Banos Alhama de Granada | BAG | S | | 40 | 7.4 | 1.13 | 2.44 | 1.30 | 1.45 | 0.15 | 3.59 | 1.39 | 2.05 | 0.55 | 6.85E-04 | 3.49E-04 | b.d.l | 0.04 | 0.67 | 0.02 |
| 37°01.1221'N; 3°58.9970'W | | | | | | | | | | | | | | | | | | | | |
| Banos Nuevo Alhama de Granada | BNAG | S | | 39 | 7.2 | 1.24 | 2.63 | 1.36 | 1.87 | 0.17 | 2.89 | 1.89 | 2.60 | 0.72 | 6.95E-04 | 2.71E-04 | 4.42E-04 | 0.06 | 0.73 | 0.08 |
| 37°01.3410'N; 3°58.7548'W | | | | | | | | | | | | | | | | | | | | |
| Alicun de las Torres | AT | S | | 34 | 6.7 | 2.24 | 8.25 | 4.35 | 2.32 | 0.12 | 2.06 | 2.32 | 11.4 | 0.31 | 8.89E-04 | 1.38E-04 | b.d.l. | 0.11 | 1.83 | 0.87 |
| 37°30.5418'N; 3°06.4172'W | | | | | | | | | | | | | | | | | | | | |
| Banos de Zujar | BZ | W | - | 35 | 6.8 | 12.8 | 15.8 | 8.01 | 56.1 | 0.62 | 2.91 | 61.4 | 23.3 | 0.62 | 1.71E-02 | 1.98E-04 | 5.74E-03 | 0.23 | 6.80 | 3.03 |
| 37°34.556'N, 2°49.463'W | | | | | | | | | | | | | | | | | | | | |

Table 1: Sample details including sample location and water chemistry. Location of sampling points refer to WGS84 system. Type of water points: S = spring; W = well. EC is electrical conductivity in mS/cm. Concentrations of dissolved elements and TDS are expressed in mmol/kg of solution and in mg/L respectively. CBE (Charge Balance Error) is expressed in %. b.d.l = below detection limit.

| Sample | Calcite | Dolomite | Gypsum | Anhydrite | Halite | Quartz | Chalcedony | K-feldspar | Kaolinite | Albite | Anorthite | Ca-Mont. | $CO_2$(g) | $fCO_2$(g) |
|---|---|---|---|---|---|---|---|---|---|---|---|---|---|---|
| ***Contacts metam. complexes*** | | | | | | | | | | | | | | |
| BSL | -0.61 | -1.39 | -1.40 | -1.61 | -4.66 | 1.14 | 0.74 | 3.15 | 8.02 | 1.65 | -1.03 | 7.96 | 0.01 | 1.03 |
| CL | 0.32 | 0.34 | -0.63 | -0.86 | -3.21 | 1.25 | 0.83 | 5.42 | 10.44 | 3.90 | 1.93 | 11.01 | -0.02 | 0.96 |
| BAA | 0.02 | 0.27 | -1.83 | -1.89 | -6.17 | 0.74 | 0.42 | 0.14 | 2.52 | -0.52 | -2.79 | 1.65 | -1.21 | 0.061 |
| ***Graben into Alp. Complex*** | | | | | | | | | | | | | | |
| BUC | 0.41 | 0.75 | -1.19 | -1.42 | -8.46 | 0.40 | -0.01 | -0.67 | 3.23 | -2.31 | -2.68 | 1.90 | -2.23 | 0.006 |
| BUG | 0.16 | 0.23 | -1.21 | -1.44 | -6.52 | 0.37 | -0.05 | 0.18 | 4.36 | -1.25 | -2.25 | 3.05 | -1.95 | 0.011 |
| ***Evaporitic basin*** | | | | | | | | | | | | | | |
| BM | 0.43 | 0.78 | -0.37 | -0.57 | -6.33 | 0.54 | 0.15 | 0.56 | 4.06 | -0.57 | -1.42 | 3.14 | -2.22 | 0.006 |
| SF | 0.21 | 0.34 | -0.07 | -0.22 | -6.13 | 0.48 | 0.12 | 0.37 | 4.18 | -0.73 | -1.20 | 3.23 | -1.79 | 0.016 |
| SRN | 0.39 | 0.74 | -0.06 | -0.25 | -5.35 | 0.52 | 0.14 | 1.15 | 5.12 | 0.25 | -0.35 | 4.34 | -2.10 | 0.008 |
| SE | 0.04 | 0.07 | -0.43 | -0.63 | -5.65 | 0.52 | 0.13 | 0.91 | 5.65 | 0.00 | -0.81 | 4.81 | -1.60 | 0.025 |
| BAG | 0.32 | 0.62 | -1.30 | -1.44 | -7.41 | 0.48 | 0.12 | -0.39 | 2.49 | -1.80 | -2.54 | 1.31 | -1.95 | 0.011 |
| BNAG | 0.06 | 0.06 | -1.18 | -1.33 | -7.17 | 0.61 | 0.25 | 0.07 | 3.20 | -1.29 | -2.26 | 2.24 | -1.87 | 0.013 |
| AT | -0.32 | -0.73 | -0.37 | -0.55 | -7.03 | 0.31 | -0.06 | -0.83 | 4.02 | -1.99 | -2.45 | 2.63 | -1.63 | 0.024 |
| BZ | 0.01 | -0.07 | -0.10 | -0.27 | -4.32 | 0.62 | 0.25 | 2.00 | 6.90 | 1.52 | 0.84 | 6.46 | -1.62 | 0.024 |

Table 2: Saturation indices (SI) of the main mineral phases of interest in the investigated area. $CO_2$(g) corresponds to the log10 of $CO_2$ fugacity ($fCO_2$). SI were calculated with the PHREEQC code at the outlet temperature (measured in the field).

| Sample | $O_2$ cc/L | $N_2$ cc/L | $CO_2$ cc/L | $pCO_2$ atm | $H_2$ ppm | CO ppm | $CH_4$ ppm | TDIC mmol/L | $\delta^{13}C_{(TDIC)}$ ‰ | $\delta^{13}C_{(CO2)}$ ‰ |
|---|---|---|---|---|---|---|---|---|---|---|
| ***Contacts metam. complexes*** | | | | | | | | | | |
| BSL | 0.07 | 1.74 | 576 | 0.78 | 6.82E-04 | 2.88E-04 | 5.29E-03 | 46.6 | -5.2 | -6.6 |
| CL | 0.08 | 1.94 | 597 | 0.71 | b.d.l | 1.41E-04 | 8.66E-05 | 63.0 | -4.7 | -7.5 |
| BAA | 1.49 | 12.1 | 39.4 | 0.088 | 9.72E-04 | 3.16E-04 | 1.53E-02 | 9.1 | -9.0 | -13.6 |
| ***Graben into Alp. Complex*** | | | | | | | | | | |
| BUG | 1.57 | 18.6 | 16.2 | 0.020 | b.d.l | 2.69E-05 | 6.36E-04 | 4.6 | -9.0 | -16.2 |
| ***Evaporitic basin*** | | | | | | | | | | |
| SF | 1.81 | 17.0 | 9.51 | 0.017 | b.d.l | 3.51E-05 | 1.38E-02 | 2.9 | -1.5 | -6.6 |
| SE | 0.13 | 18.3 | 22.2 | 0.033 | b.d.l | b.d.l | 2.39E-04 | 4.5 | -8.8 | -14.5 |
| BAG | 0.67 | 17.6 | 10.7 | 0.020 | b.d.l | b.d.l | 7.43E-04 | 3.8 | -7.6 | -13.3 |
| AT | 0.44 | 16.7 | 27.0 | 0.044 | 1.10E-03 | 7.03E-05 | 2.48E-05 | 2.7 | -5.0 | -9.8 |
| BZ | 0.62 | 13.8 | 16.3 | 0.027 | 1.51E-03 | 2.02E-04 | 3.37E-02 | 3.5 | -3.4 | -8.4 |

Table 3: Dissolved gases and carbon isotopic composition of the selected investigated thermal waters. TDIC was calculated using PHREEQC. b.d.l = below detection limit.

| Sample | Outlet temp. | $SiO_2$-Quartz | | | | $SiO_2$-chalcedony | | Ca/Mg | $fCO_2$ |
|---|---|---|---|---|---|---|---|---|---|
| | | Michard (1979) | Verma (2000b) | Fournier and Potter (1982) | Fournier (1977) | Arnorsson (1983) | Michard (1990) | Chiodini (1995a) | Chiodini (1995a) |
| ***Contacts metam. complexes*** | | | | | | | | | |
| BSL | 26 | 145 | 143 | 146 | 139 | 115 | 102 | 86 | 16.34 |
| CL | 21 | 133 | 130 | 134 | 129 | 103 | 92 | 88 | 23.82 |
| BAA | 51 | 128 | 124 | 128 | 127 | 97 | 87 | 60 | 5.63 |
| ***Graben into Alp. Complex*** | | | | | | | | | |
| BUC | 25 | 57 | 47 | 57 | 62 | 26 | 24 | 75 | 0.54 |
| BUG | 23 | 52 | 42 | 51 | 58 | 21 | 20 | 74 | 0.66 |
| ***Evaporitic basin*** | | | | | | | | | |
| BM | 30 | 76 | 67 | 76 | 79 | 45 | 41 | 81 | 0.08 |
| SF | 39 | 83 | 74 | 83 | 85 | 52 | 47 | 87 | 0.05 |
| SRN | 32 | 76 | 67 | 76 | 79 | 45 | 41 | 75 | 0.04 |
| SE | 30 | 74 | 66 | 75 | 78 | 43 | 40 | 71 | 0.16 |
| BAG | 40 | 84 | 76 | 85 | 86 | 53 | 48 | 89 | 0.74 |
| BNAG | 39 | 96 | 89 | 97 | 97 | 65 | 59 | 91 | 0.38 |
| AT | 34 | 61 | 52 | 61 | 66 | 30 | 28 | 88 | 0.05 |
| BZ | 35 | 90 | 82 | 90 | 91 | 58 | 53 | 84 | 0.06 |

Table 4: Temperature (°C) obtained with selected geothermometers and fugacity of $CO_2$ ($fCO_2$) obtained with Chiodini et al. (1995a)'s geobarometer.

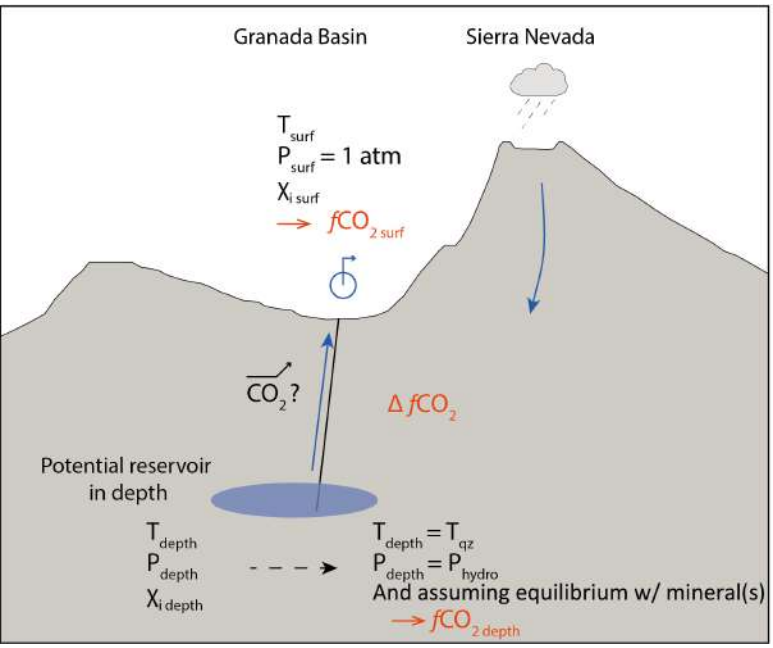
Granada Basin
Sierra Nevada
T surf
P surf = 1 atm
X i surf
→ fCO2 surf
CO2 ?
Δ fCO2
Potential reservoir
in depth
T depth
P depth
X i depth
T depth = T qz
P depth = P hydro
And assuming equilibrium w/ mineral(s)
→ fCO2 depth

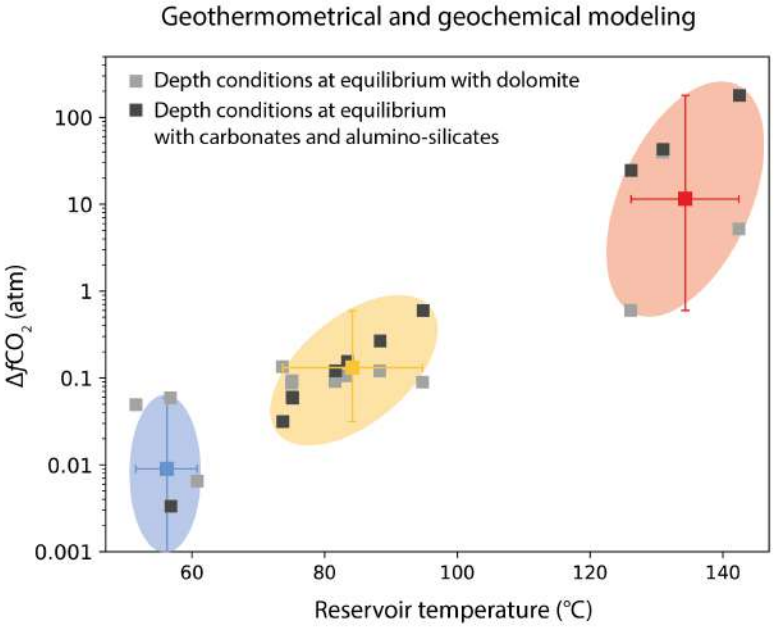
Geothermometrical and geochemical modeling
Depth conditions at equilibrium with dolomite
Depth conditions at equilibrium
with carbonates and alumino-silicates
ΔfCO2 (atm)
100
10
1
0.1
0.01
0.001
60
80
100
120
140
Reservoir temperature (°C)